

Climatology of Radiation Budget Measurements from Satellites

by
G.G. Campbell and T.H. Vonder Haar

Department of Atmospheric Science
Colorado State University
Fort Collins, Colorado

February 1981

**Colorado
State
University**

**Department of
Atmospheric Science**

Paper No. 323

CLIMATOLOGY OF RADIATION BUDGET MEASUREMENTS
FROM SATELLITES

by

G. G. Campbell and T. H. Vonder Haar

Department of Atmospheric Science
Colorado State University
Fort Collins, Colorado 80523

February 1980

Atmospheric Science Paper No. 323

ABSTRACT

Forty eight months of broadband earth radiation budget measurements have been accumulated into a climatology from satellite experiments. Monthly maps with 1100 km (10^0) resolution are presented for the emitted flux, albedo and net radiation. The incident solar radiation is the prime determinant of the net radiation budget with land ocean distribution being the next significant factor. Mean cloudiness has an obvious effect on the mean net radiation only in a few places although cloud changes do have large effects on the albedo and emitted exitance. The zonal average ocean budget components are almost perfectly symmetric about the equator (with a six month shift). However, the land zonal average is much different than the ocean showing the need for consideration of land-ocean differences even in the simplest climate models. Several regional radiation budgets are discussed in detail.

TABLE OF CONTENTS

	<u>Page</u>
Abstract	i
Introduction	1
Error Estimates.	6
Annual and Zonal	9
Zonal Land/Ocean	19
Extremes	25
Relative Dispersion.	25
Monthly Maps	31
Regional Studies	32
Longitude Sections.	32
Particular Regions.	37
Conclusions.	39
Credits.	42
References	43
Maps	45
Annual.	46
Monthly	48
Relative Dispersion	72
Overlay and Land/Ocean Grid.	74

Introduction

The radiative exchange between the earth and the sun and space provides the fundamental driving force for the atmosphere-ocean circulation. This was first suggested by Dines (1917). There were several ground based estimates of the components of the radiation budget (Simpson, 1927; London, 1957) but satellites made it possible to measure the exchange directly. The more recent motivation for measuring the details of the radiation fields are to understand more of the feedbacks in the circulation system (Earth Radiation Budget Science, 1978). There have been several publications on features of the monthly zonal averages (Table 1), and a few studies of geographical variation, considering both east-west, as well as north-south patterns. The last 17 years have seen several earth satellite experiments to measure the large scale features of this radiative exchange. The Nimbus 6 Earth Radiation Budget experiment has ushered in a new era of measurements with a continuous time series beginning in July, 1975. This has been continued to the present with the Nimbus 7 experiment. Here we analyze a summary of the broad band radiation data including 48 months of observations extant today.

This study doubles the previous data considered in studies of the two dimensional (latitude and longitude) monthly budget, and now can be considered almost a long term climatology. This is a continuation of the radiation budget climatologies from satellites begun by Vonder Haar and Suomi (1971), Vonder Haar (1972) and Vonder Haar and Ellis (1974). As more observations are made and processed, deviations from this climatology may reasonably be compared to their long term average "climate". A similar climatology, using different data is that

Table 1
Radiation Budget Climatologies From Satellite Observations

Zonal Average	Comments
1. Winston, 1971	Monthly zonal averages discussed
2. Vonder Haar, 1972	Albedo 1967 observations from digitized photographs
3. Ellis and Vonder Haar, 1976	Summary of 29 months from several satellite systems
4. Jacobowitz, 1979	18 months of Nimbus 6 observations
Latitude and Longitude (Maps)	
1. Vonder Haar and Suomi, 1971	Seasonal results
2. Vonder Haar and Ellis, 1974	17 seasons and some monthly
3. Winston et al., 1979	43 months of NOAA scanning radiometer data (4 different satellites)

by Winston et al., 1979. This used nearly 4 years of NOAA scanning radiometer results but their instruments had a limited spectral range and thus did not measure the total energy exchange between earth and space.

We will discuss many of the important features in the radiation budget climatology emphasizing the geographic dependence of the time variation. It is likely that we will have missed some significant features so the reader is welcome to search the data for other events. Part of the reason for presenting this atlas with its great number of maps is just the possibility of others finding important results.

The emitted radiant exitance and the albedo at the top of the atmosphere are the fundamental analyzed measurements of all these

experiments. From these two one can derive the net gain of energy of earth system (Eq. 1) - the real dynamical driving force of the atmosphere and ocean.

$$\begin{aligned} \text{Net} &= \text{Incident} - \text{Reflected} - \text{Emitted} \\ &= \text{Incident} (1-\text{Albedo}) - \text{Emitted} \end{aligned} \tag{1}$$

For consistency, we have used the Nimbus 7 observations of the solar constant, 1376 w/m^2 (Hickey et al., 1980) in calculating the average incident flux for each month. All of the individual observations for each month were averaged to produce a monthly mean map. The mean maps were then averaged to produce the annual maps. Note also that the albedo was not averaged but was recalculated from the ratio of the mean reflected flux to the mean incident flux.

Six different experiments contributed to the results presented here. Table 2 shows a listing of these systems and their local time of measurement. The measurements were of variable accuracy and resolution but we use this variety to give better local time sampling to the overall climatology. The diameter of the half power field-of-view region is a measure of the spatial resolution of the particular system and is also listed in Table 2.

The so-called experimental satellite data were measurements made from radiometers flown on several satellites in the early 1960's, (Vonder Haar and Suomi, 1971). Two flat plate spatially integrating radiometers were used in conjunction - a black painted detector responding to all light incident and a white painted detector which absorbed only the emitted exitance from the earth. This is typical of several of these radiometer systems which require a difference between measurements

to determine one of the spectral intervals. In this case the reflected is the total minus the emitted. The albedo is then determined by estimating the maximum reflected flux from a diffuse reflecting earth and dividing that into the measured reflected flux. The top-of-the-atmosphere emitted exitance is determined from the emitted exitance measured with a simple distance correction.

The ESSA3 and ESSA7 measurements were recorded from flat plate detectors which were located on a rolling satellite (spin axis parallel to orbit angular momentum) (MacDonald, 1970). The most serious problem here was the need to assume monthly global radiation balance to get an inflight calibration. This fact and the low resolution of these instruments indicates that these data should be deleted from the mean when several more years of data and measurements at these local times become available in the future.

The Nimbus 2 and Nimbus 3 measurements are inherently different than the others because they were made with scanning instruments with narrow fields of view (Raschke and Bandeen, 1970, Raschke et al., 1973). The scanning radiances were converted to top-of-the-atmosphere albedo using complicated bidirectional and directional reflectance models. Similarly a limb darkening model was used to analyze the emitted radiances. The 250 km resolution gridded data was changed to 10^0 resolution maps by a simple area average.

The Nimbus 6 Earth Radiation Budget wide field of view data was analyzed by us in a rather complicated fashion to enhance the spatial resolution (Campbell and Vonder Haar, 1980). Jacobowitz (1979) discussed several features of the zonal mean and global mean Nimbus 6 data from a separate analysis. The flat plate thermopiles consisted of a

total spectral sensor (black) and Suprasil-W filter sensor detecting only reflected flux from the earth. Smith et al. (1975) give a complete discussion of the instruments. A deconvolution scheme (Smith, Greene and Campbell, 1976) was used to enhance the original resolution of 16° to 10° for both the emitted flux and albedo estimates. In addition, the albedo results have been processed with the Nimbus 3 directional reflectance model to partially remove the diurnal bias of observations near local noon. These measurements promise to continue in the future with 16 more months of Nimbus 6 and more than 1 year of Nimbus 7 recorded to date.

Table 2. Experiments Included
(Local time of observations)

Month	1964	1965	1966	1968	1969	1970	1975	1976	1977
1		Ex(10:30)			E7	N3		N6	N6
2		Ex(10:35)			E7			N6	N6
3		Ex(10:40)			E7			N6	N6
4					N3(11:30)*			N6	N6
5					N3			N6	N6
6			N2(11:30)*		N3			N6	N6
7	Ex(8:30)				N3		N6(11:45)*	N6	
8	Ex(8:55)				N3		N6	N6	
9	Ex(9:15)						N6	N6	
10	Ex(9:40)			E7(14:30)	N3		N6	N6	
11	Ex(10:05)				E7		N6	N6	
12	Ex(10:30)		E3(14:30)		E7		N6	N6	

Resolution \approx Half Power Field-of-View Diameter

Experimental	1280km, 11.5°
ESSA3	
Nimbus 2	Averaged to 10° grid
ESSA7	2200km, 20°
Nimbus 3	Averaged to 10° grid
Nimbus 6	1100km, 10° (analyzed from 16°)

*Albedo corrected for diurnal variation of reflection with directional reflectance model.

Error Estimate

There are several error sources in the satellite experiments used in this set. The primary problem is the inability to compare observations of the same thing with two systems, i.e., overlapping measurements in space and time are not available. The other major problem is the lack of absolute calibration of the instruments, allowing systematic errors. An additional source of uncertainty is the natural variability of the weather and the possibility that we have not sampled enough years.

The relative errors are smaller than the possible systematic errors so the spatial patterns shown in the maps are likely to be correct. But the numbers presented may be inaccurate because of systematic offsets between the measuring systems and reality. Below we will attempt to estimate the quantitative errors but this is difficult because there are no multiple simultaneous measurements in time and thus one cannot use the variance as an error estimator. Ellis and Vonder Haar discussed this in "Zonal Average Earth Radiation Budget Measurements from Satellites for Climate Studies" (1976). We have made some improvement, at least in the relative sense, with more measurements.

The solar insolation is no longer in doubt, being $1376 \pm 1 \text{ W/m}^2$ with no variation in time from 1975 to 1979 (Hickey et al., 1980). Whether this was the insolation before 1975 is unknown, but is an accurate assumption.

Some error sources relate mostly to systematic errors, which are unlikely to affect the pattern in the maps:

1. Absolute calibration difficulties
2. Sensor degradation in space with time

3. The ESSA7 data were analyzed with the assumption that net radiation was zero on a monthly basis.
4. Data gaps appear in the record so that a reported monthly mean sometimes represents less than half the month.

Other error sources affect the absolute value and the patterns and thus are more serious;

5. Spatial smoothing due to the integrating nature of most of the instruments. This limits the resolution to, at best, 10° great circle arc with large discontinuation smoothed out even at that resolution. A displacement of 10° will change the information by 50%. Thus there is still a high correlation between adjacent points due to the measurement system.
6. Diurnal sampling bias results from the sun synchronous nature of all these measuring systems. The local time of observation is constant for each system and at each latitude, but it shifts as one moves north or south. This could produce shifts in the north-south pattern especially in the polar regions. The more serious problem is the systematic bias produced by not sampling all the possible weather events during the day.
7. Angular reflection models were used in the analysis of the Nimbus 2 and 3 to transform the scanner radiance measurements to flux estimates. This also adjusted the local noon measurements to daily average. These models are not highly accurate.
8. Angular reflection models were used in the analysis of Nimbus 6 results primarily to adjust for the local noon observation time. A very serious diurnal bias can occur with local noon measurements because of the systematic increase of reflection coefficient with increasing sun angle.
9. Because of satellite recording problems only daytime emitted measurements are available for the two years of Nimbus 6.
10. The number of samples limits the accuracy with only 4 or 5 observations each month. But beyond monthly averages (i.e. seasonal or annual) one is limited by systematic errors not random ones.

Our estimate of the absolute accuracy of any individual month is still $\pm 5\%$ (Ellis and Vonder Haar, 1976). The relative accuracy is better though, probably $\pm 3\%$ emitted and $\pm 4\%$ albedo. Table 3 shows our current estimate of the accuracy of the net flux for any month. This has been prepared by combining the errors as if they were random (Eq. 2).

Table 3. Monthly uncertainty of net

J	F	M	A	M	J	J	A	S	O	N	D	ANNUAL
4.1	I	4.3	7.9	12.6	15.6	9.8	7.9	6.5	I	4.7	4.4	7.2
I	4.3	4.9	8.7	11.6	12.2	7.8	7.4	7.5	4.4	I	3.9	6.9
4.1	4.9	5.7	9.1	10.4	10.6	7.1	7.4	7.7	4.8	5.0	4.2	7.0
4.5	5.5	6.4	9.0	9.8	10.3	7.2	7.7	8.3	5.3	5.6	4.6	7.4
5.0	6.2	6.8	9.1	9.7	10.3	7.3	8.0	9.0	5.9	6.2	5.2	7.9
5.8	7.0	7.4	9.6	9.8	10.2	7.2	8.3	9.7	6.6	7.0	5.8	8.4
6.6	7.7	7.9	10.2	10.2	10.3	7.2	8.2	10.0	7.0	7.7	6.6	8.7
7.0	8.1	8.0	10.0	9.8	9.6	6.7	7.6	9.4	6.7	7.7	6.8	8.6
6.7	7.8	7.8	9.2	9.0	9.1	6.4	7.5	9.2	6.7	7.6	6.7	8.3
6.6	7.6	7.6	9.2	9.6	9.7	6.9	8.0	9.8	6.9	7.8	6.7	8.5
6.8	7.8	7.8	9.8	9.9	10.0	7.0	8.3	10.1	7.1	8.1	7.0	8.7
7.1	8.0	7.9	9.7	9.4	9.4	6.7	7.9	9.8	7.0	8.1	7.2	8.6
7.1	8.1	7.7	8.9	8.6	8.3	5.0	7.1	9.0	6.7	8.0	7.1	8.3
7.1	7.8	7.2	8.2	7.8	7.6	5.3	6.3	8.2	6.4	7.9	7.2	7.9
7.4	7.8	6.8	7.6	6.9	6.9	4.8	5.6	7.6	6.3	8.3	7.6	7.5
7.6	7.5	6.2	6.8	6.3	6.1	4.1	4.8	6.6	6.1	8.6	8.2	7.1
8.9	7.6	5.3	5.5	I	5.2	I	3.6	5.2	5.5	9.8	9.9	6.7
9.8	7.8	4.4	I	3.7	3.9	2.6	I	3.3	4.8	10.8	11.4	6.3

Monthly average errors assuming $\pm 5\%$ emitted and $\pm 5\%$ albedo treated as random errors, eq. 2. The annual column was estimated assuming $\pm 3\%$ emitted and $\pm 4\%$ albedo systematic errors, so the number of samples did not decrease the final error.

$$\sigma_{\text{net}}^2 = (\sigma_{\text{Emitted}}^2 + \sigma_{\text{albedo}}^2 I^2) / (k-1)k \quad (2)$$

I = Incident radiant flux

k = Number of observations

σ_{net} = Standard error of net radiation

σ_{emitted} = Standard error of emitted = (.05) emitted

σ_{albedo} = Standard error of albedo = (.05) albedo

The high negative correlation between exitance and albedo has been neglected. It would reduce σ_{net}^2 if included but the systematic errors outweigh this effect.

Beyond monthly averages (i.e. seasonal or annual) the sampling or number of observations no longer limits the accuracy. In fact, if one were to assume only random errors the annual average could be claimed to have 2 W/m^2 accuracy. We estimate though, that the absolute accuracy of the annual means are $\pm 3\%$ exitance, $\pm 4\%$ albedo and thus $\pm 8 \text{ W/m}^2$ net, primarily due to systematic errors. Future experiments will attempt to overcome many of these error sources; the Nimbus 6 and Nimbus 7 overlap in time; the Earth Radiation Budget Experiment of NASA and NOAA will involve 3 satellites to measure many local times: It will make simultaneous measurements from two or more satellites allowing a much better error estimate from the comparisons; and it will also have in-flight calibrations of all instruments, probably solving the calibration unknown.

Annual and Zonal

We will discuss the results in a descending hierarchy of time and space scales. The global averages for each of the monthly maps, Fig. 1,

show the typical annual cycle as discussed by Ellis et al. (1978). It is caused primarily by changes in earth sun distance and the differences in amount of land and ocean between the northern and southern hemispheres. Fig. 2 shows the area means from 70°N to 70°S with the individual instrument results superimposed. (Because of missing data near the poles in some experiments this was not done for the global averages.) We think that the variations around the mean are most likely caused by observing system differences and to a lesser extent by weather variations because of the grouping of particular experiments on one side or the other of the mean. It is possible that the scatter is due to natural variability of the weather but this is uncertain because of the imprecise absolute calibrations. The annual, global average emitted radiant exitance is $232 \pm 7 \text{ W/m}^2$, the earth albedo is $.30 \pm .01$ and the net radiation is $9 \pm 8 \text{ W/m}^2$. We suspect that these averages contain systematic errors because a 1 W/m^2 net radiant flux would change the temperature of a 100m deep ocean layer about 0.1 K each year. If the reported net had been sustained for the 17 years of those observations its effects would likely have been seen in the ocean temperature! This indicates, for purposes of energetics studies, that the data be re-normalized to give annual global net radiation close to zero. We suggest that the albedo and emitted terms both be multiplied by 1.025 rather than adding a constant to the net. A rescaling like this is equivalent to a change in sensitivity of the detectors by 2.5%. This has not been done for this report because we prefer to present as close to the original data as possible.

The zonal (longitudinal) average seasonal variation shows many interesting features, some of which are well known (Fig. 3, Table 4).

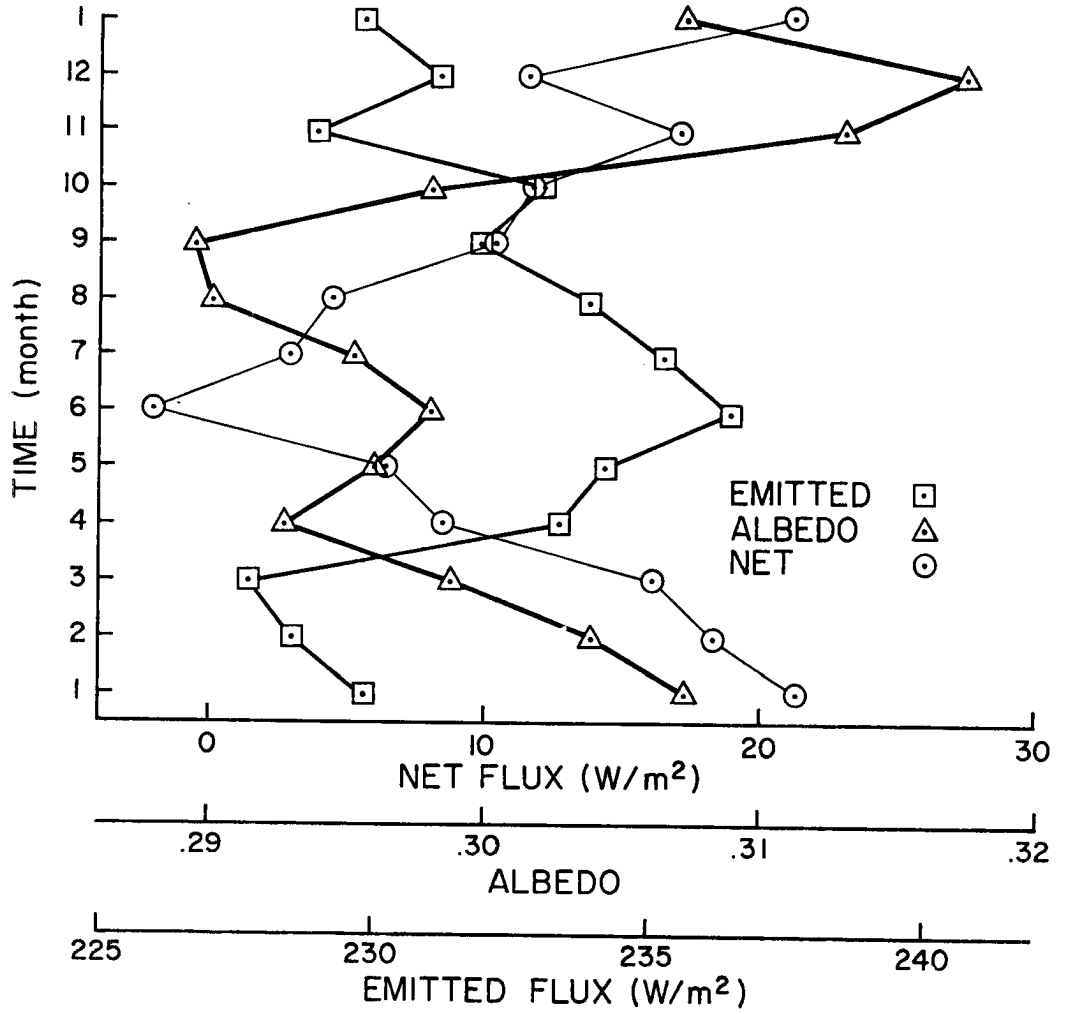


Figure 1
Global Averages

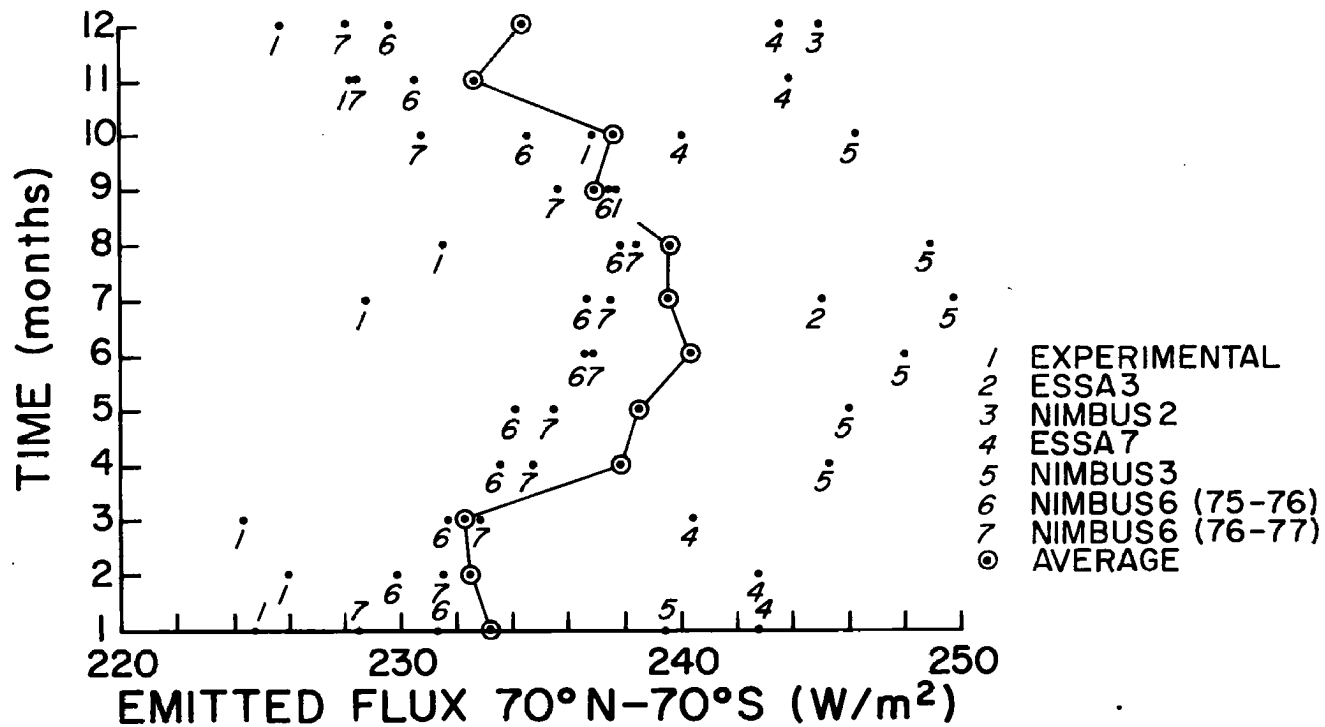


Figure 2a. Experiment Comparisons

Near global averages with the dots showing individual month measurements. The scatter is more likely caused by systematic experiment differences but some may be weather variations.

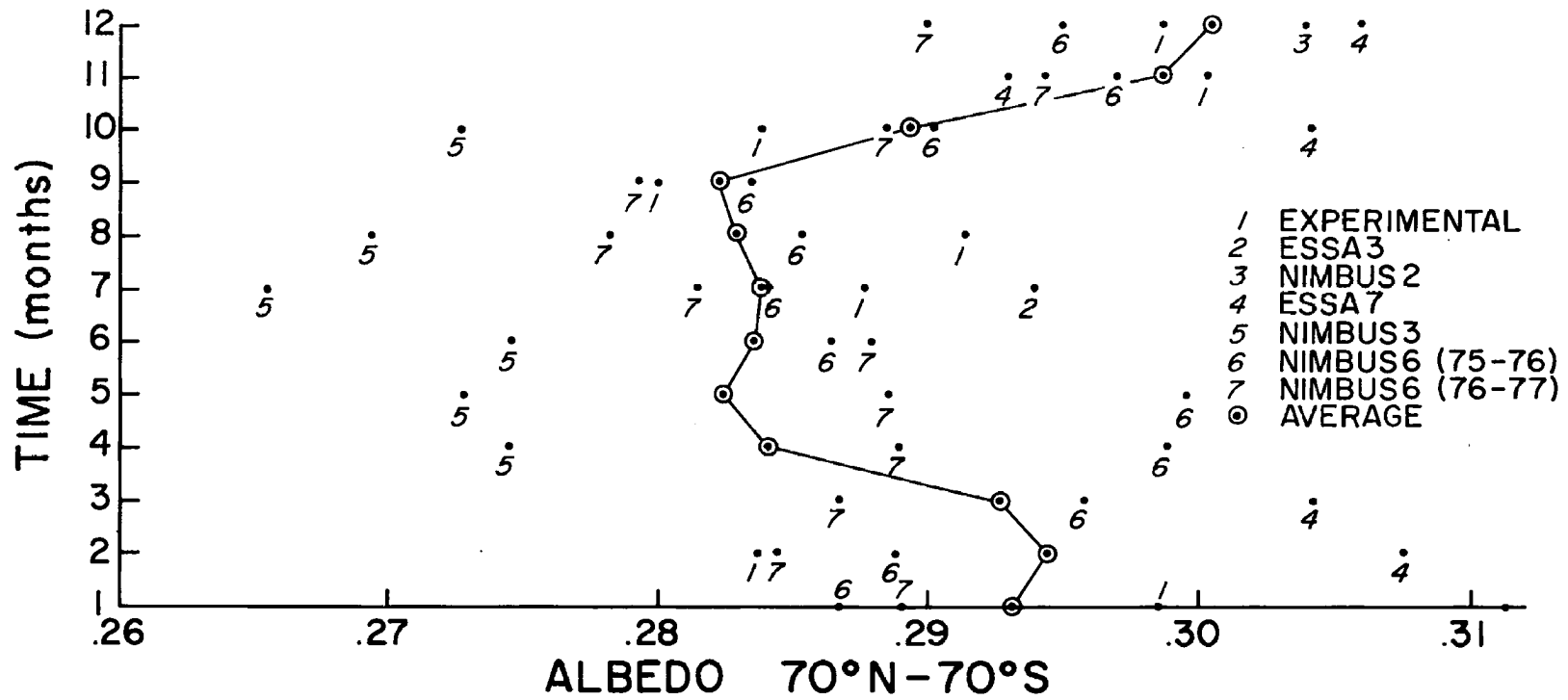


Figure 2b. Experiment Comparisons

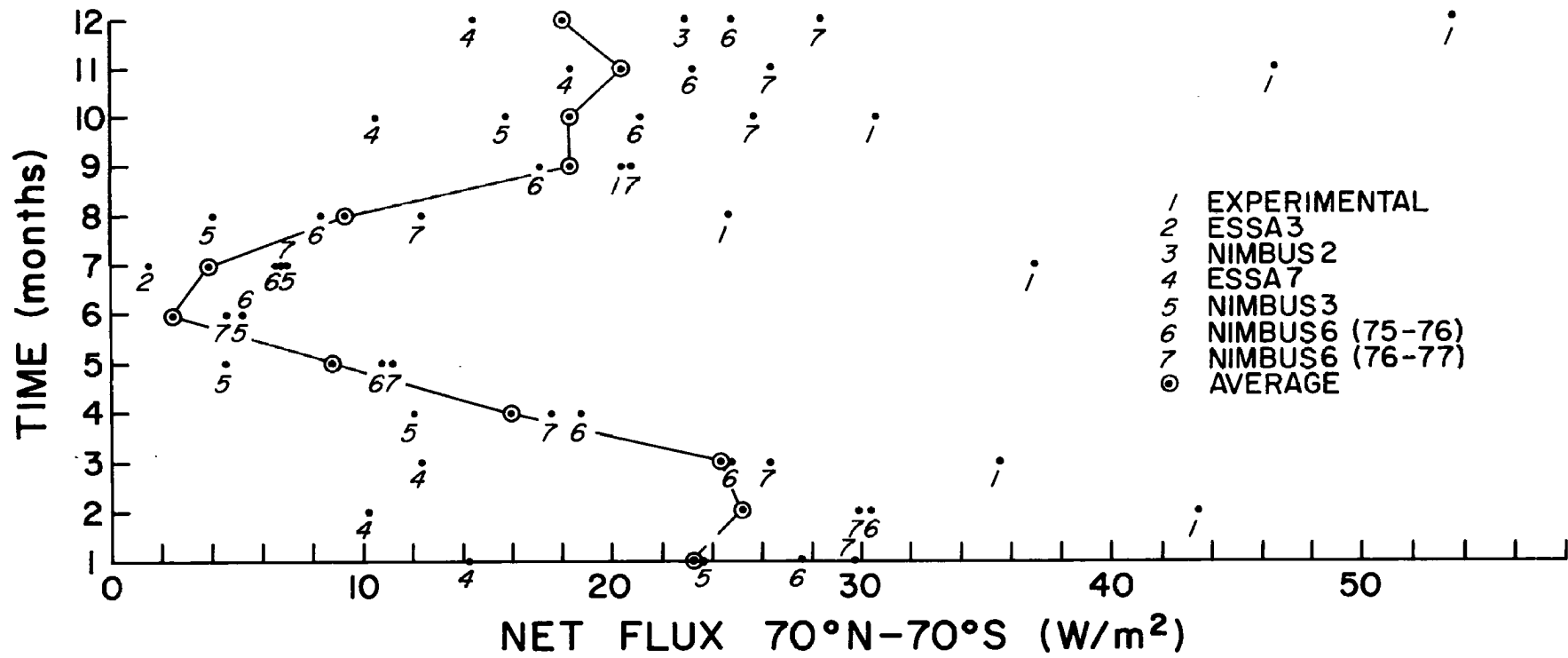


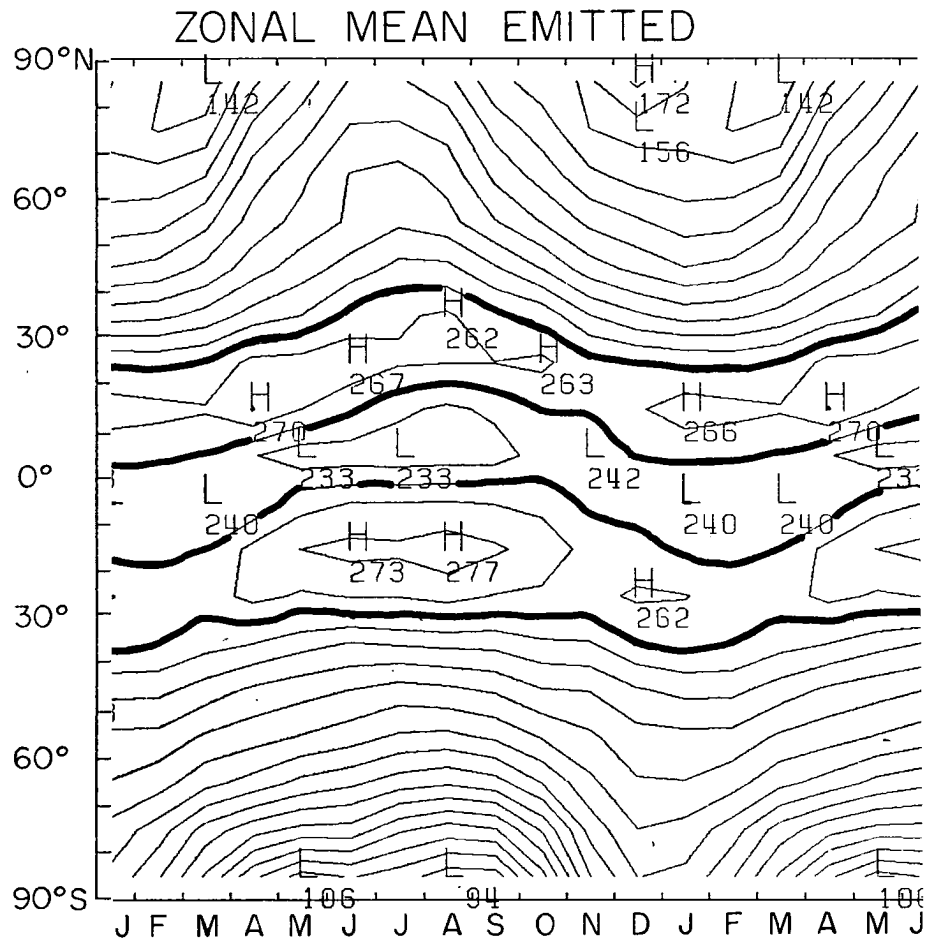
Figure 2c. Experiment Comparisons

There is an approximate symmetry between the northern and southern hemispheres if one shifts one hemisphere 6 months. This of course produces the symmetry between north and south winters and between north and south summers. The emitted radiant flux matches the observed variation in near surface temperature as one would expect (Fig. 4), although the minimum at the equator is not apparent. There are three extreme points in the zonal profiles with a minimum and maximum near the equator in both subtropics. The minimum is an indication of the cloudiness near the equator and its migration north and south with the seasons and also the cooler ocean temperatures. The highs are indications of the warm desert-like regions over both the land and ocean in the sub tropics. The annual average of the zonal means shows little of interest because it smears out the migrating minima and maxima (Fig. 8). Some other features apparent here will be explained below when the data are segregated by land and ocean.

The albedo time variation (Fig. 3b) poleward of 30° is largely caused by the change in mean sun angle. For most surfaces the albedo increases with decreasing sun angle, so for instance North America has a larger albedo in winter than summer partly because of different mean sun angles, not just because of more snow and cloudiness. Fig. 5 from Campbell and Vonder Haar (1980) shows the expected top of the atmosphere albedo variation (with time of year) for a constant surface type. This was calculated from the directional reflection models used in the Nimbus 3 analysis (Raschke et al., 1973).

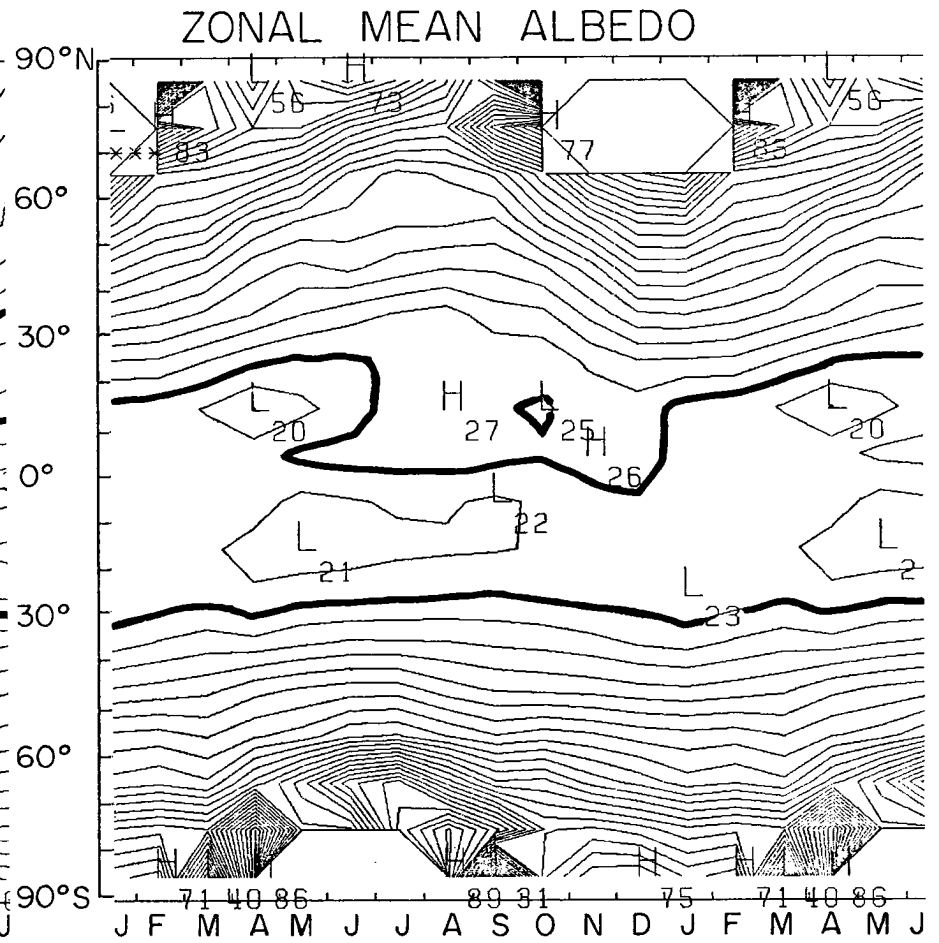
There is also a systematic increase in albedo as one moves toward the poles from the equator at any particular time of the year. This is caused more by changes in surface type (i.e. more clouds, more snow)

Figure 3a



Contour Interval 10 W/m^2
 Heavy Line at 250 W/m^2

Figure 3b

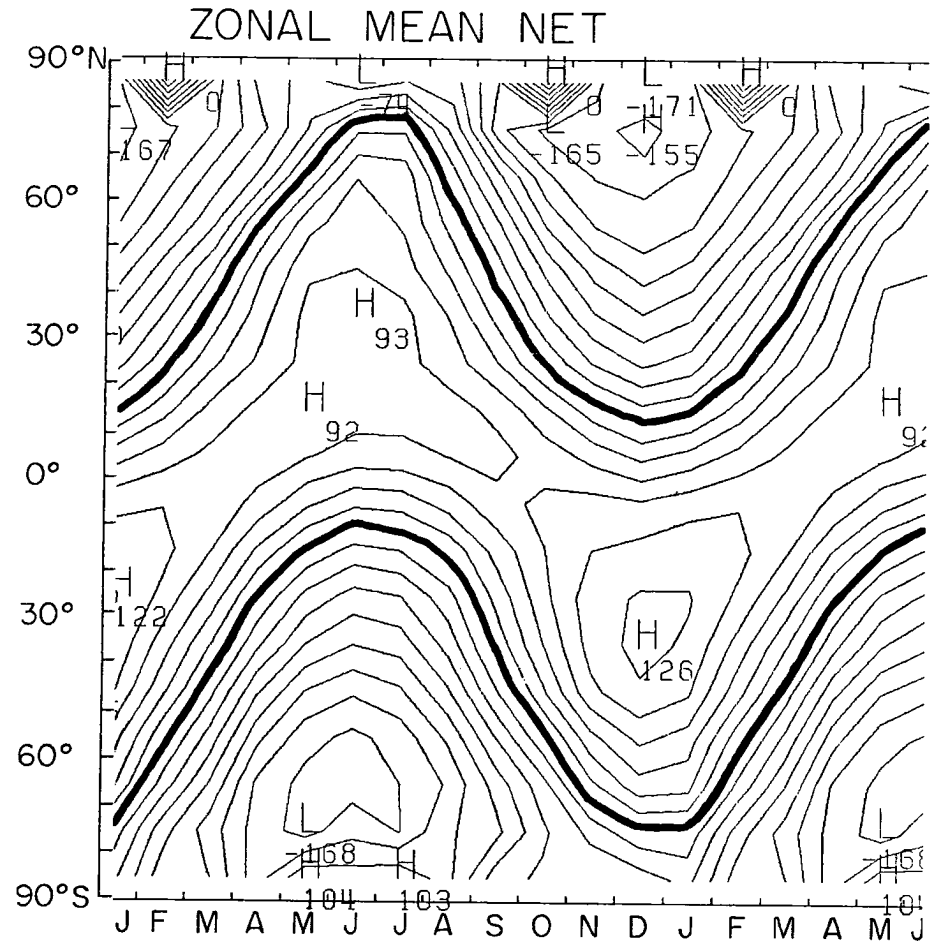


Contour Interval 2.5%
 Heavy line at 25%

TIME VARIATION

The time variation of the zonal means shows the seasonal change following the solar declination. 18 months are shown, 13-18 being a repetition of 1-6.

Figure 3c



TIME VARIATION

Contour Interval 20 W/m^2

Heavy line at 0 W/m^2

although the mean sun angle effect causes some of it. In the tropical regions the changes are caused by weather changes. The higher albedo north of the equator after May is caused by the Monsoon cloudiness.

The variation in the net is dominated by the variation in solar insolation. One might expect for a sphere with small heat capacity and conductivity that the net would always be near zero. Alternately for a large heat capacity and conductivity one would expect constant temperature and thus constant emission (in space and time). A third possibility is a system with large heat capacity but low conductivity where the temperature and emission would be constant at each latitude and there would be a large variation in the net. The earth system is near this third case but with a "medium" conductivity, so that energy transports and storage are both important. One can also see that there is a larger net before the summer solstice than after it. This indicates that the system is heating up in the spring and cooling off in the fall. This is also seen in the fact that the temperature maximum occurs about one month after the maximum net. The difference between the maximum nets between northern and southern hemispheres is best explained by land/ocean differences (see below).

The annual mean maps (Map 1) show a smoothed out version of the radiation budget showing the very zonal character of the annual climate. The major east-west variations correlate very well with land-ocean boundaries. The only oceanic "discontinuity" is the one near 180°E just north and south of the equator. The exitance shows a purely zonal character poleward of 30° except for a dip in east Asia. This zonality is just a measure of the very strong east west transport of energy by the atmosphere. In the tropics there are three major low regions; Africa,

South America and the very large region south of Asia and north of Australia. The rest of the region is an interconnected high above 240 W/m^2 . Interestingly, the two continental lows cause a lower net than the zonal mean whereas the largely oceanic low causes a high gain region. These three regions are caused by clouds as confirmed by the higher albedo in these regions.

The albedo is negatively correlated with the exitance in the tropical regions except in the Sahara, Arabian desert, over China and weakly in the North American desert. There are also many variations with geography in the Northern mid latitudes.

The reciprocity between emitted and reflected radiant flux over the ocean produces an annual net map with much more zonal character. The three wave patterns in the Southern Hemisphere (at 20-30 south) is excited by the land-ocean distribution. The S. American wiggle in the net is augmented by the stratus clouds off the west coast. (This may be true off the west coast of Africa also but instrument resolution may have smoothed this out in the annual map.) There is a large net gain region east of Africa extending all the way to S. America. Apparently mixed clouds have little effect on the net except over land as seen by those near southeast Asia. But the low stratus off the S. American coast decreases the net. The high albedo of the deserts and high emission cause lower nets, in fact a net loss over the Sahara. The whole region inside the heavy line gains energy which must be transported out by ocean or atmosphere; Oort and Vonder Haar (1976) have discussed this.

Zonal Land/Ocean

As one sees in the annual maps, there is a substantial difference between land and ocean. To examine this in more detail we have constructed

MODEL PREDICTION OF ALBEDO FOR CONSTANT SURFACE TYPE

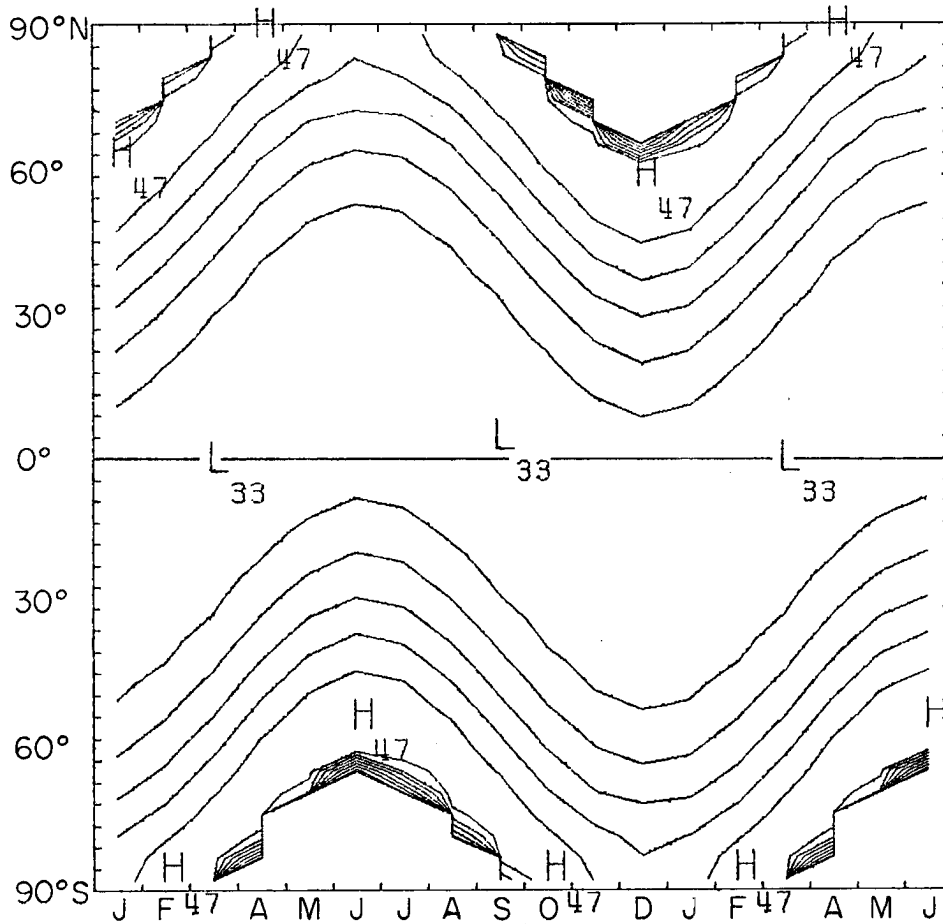


Figure 5

Model predicted albedo for a surface with 33% at the equator on the equinox. Based on the Nimbus land-cloud model (Raschke et al., 1973, Campbell and Vonder Haar, 1980). Contour interval 2.5%

the zonal average for land and for ocean (Figs. 6 and 7) which are comparable to Fig. 3. The ocean net (Fig. 6c) is much more symmetric than the land. The difference in the maxima between north and south occurs because of less insolation in June and July than in December and January with the earth-sun distance variation.

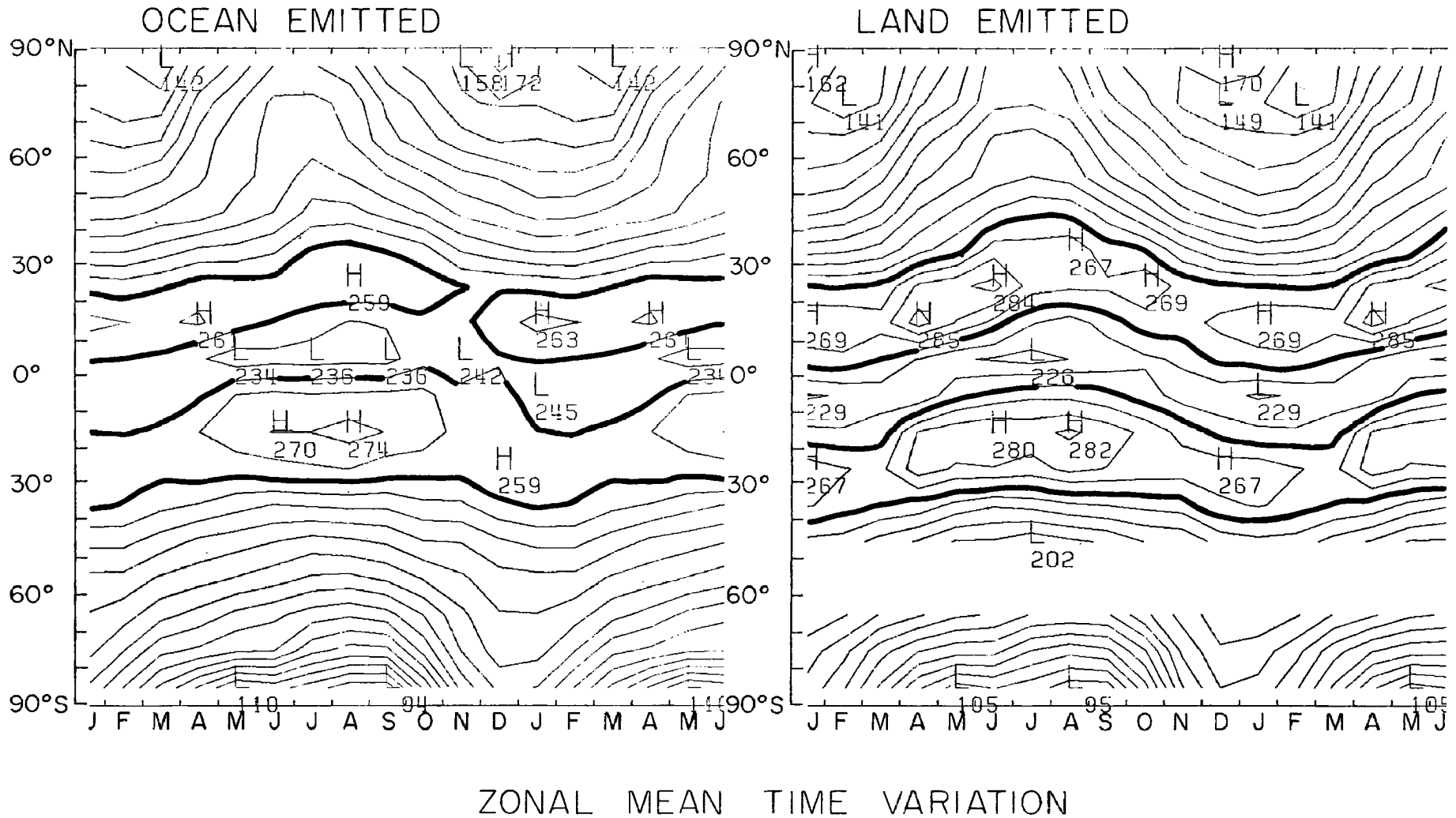
The land variation is substantially different than the ocean in the northern hemisphere in the summer, first because of the large desert regions around 30°N , these deserts gain much less energy (70 W/m^2 at the maximum in June) than the ocean both because of a higher albedo and a higher emission. Farther north (40° - 60°) the land gains more energy than the ocean in the summer because of the lower land albedo! This must be caused by clouds over the ocean since clear ocean has in general a lower albedo than most land surfaces. The southern hemisphere land is ambiguous because there is very little land south of 30°S beyond Antarctica.

The zonal average exitance over land (Fig. 7a) is very symmetric with an annual north-south migration of the three extremes. The migration must be caused by clouds near the equator and the seasonal change in the deserts at 30° . The annual average smooths this out showing the biasing produced by time averages. The ocean pattern (Fig. 6a) is less distinct because the temperature variation from 30° - 40° is less over the ocean than over the land deserts.

The albedo land, ocean zonal variation is more complex (Fig. 6b and 7b). The appearance of the monsoon causes the increased albedo north of the equator from June to October both over the ocean and land. The high albedo over the ocean just north of the equator in November and December is quite curious but we have no immediate explanation. One sees from

Figure 6a

Figure 7a

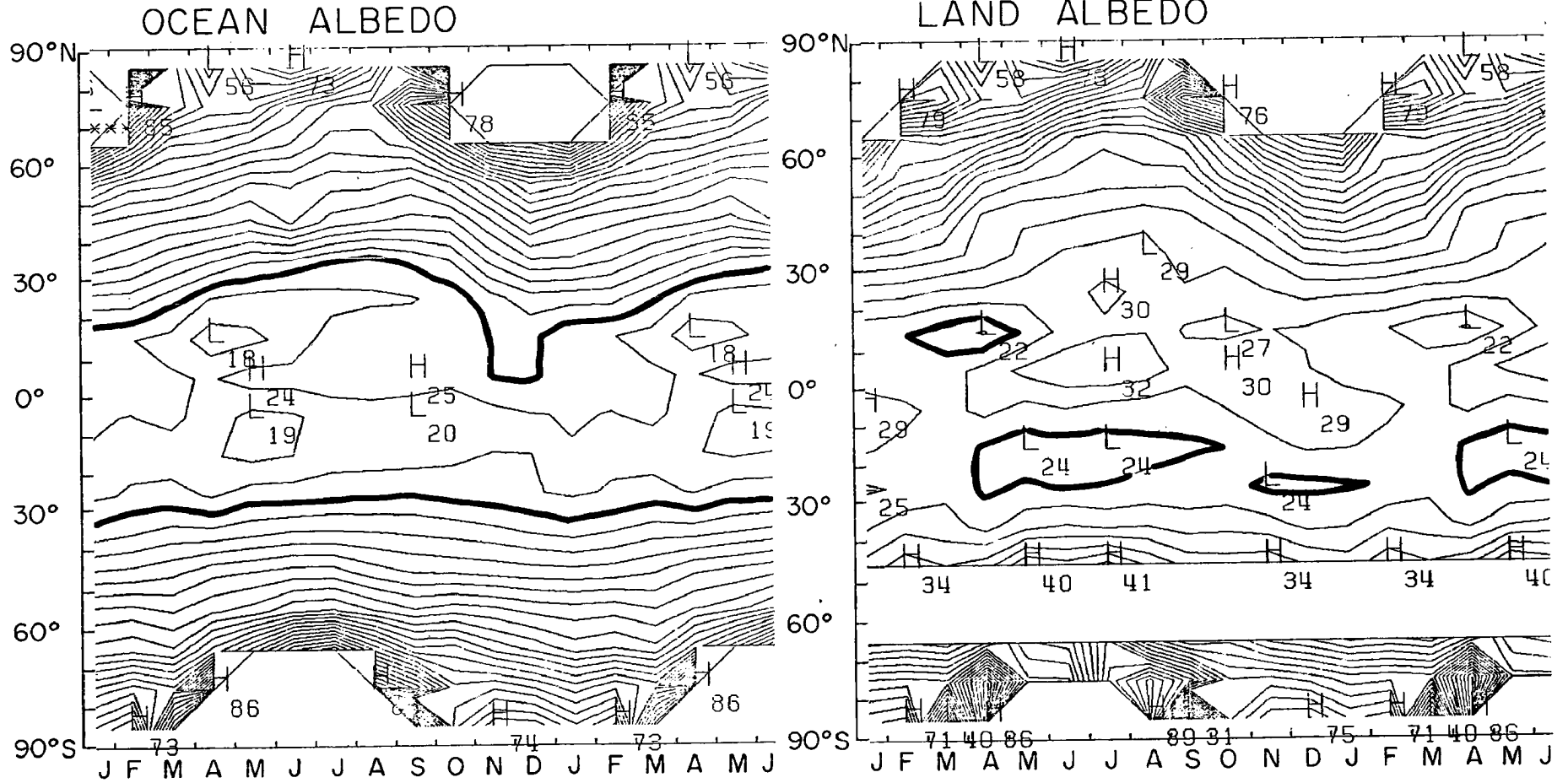


Figures 6a & 7a. Contour interval 10 W/m^2 . Heavy line at 250 W/m^2 .

Figures 6 and 7 contrast the mean ocean and mean land parameters. The blank region in the land plots appears because there is insignificant land between 45° and 65° south.

Figure 6b

Figure 7b

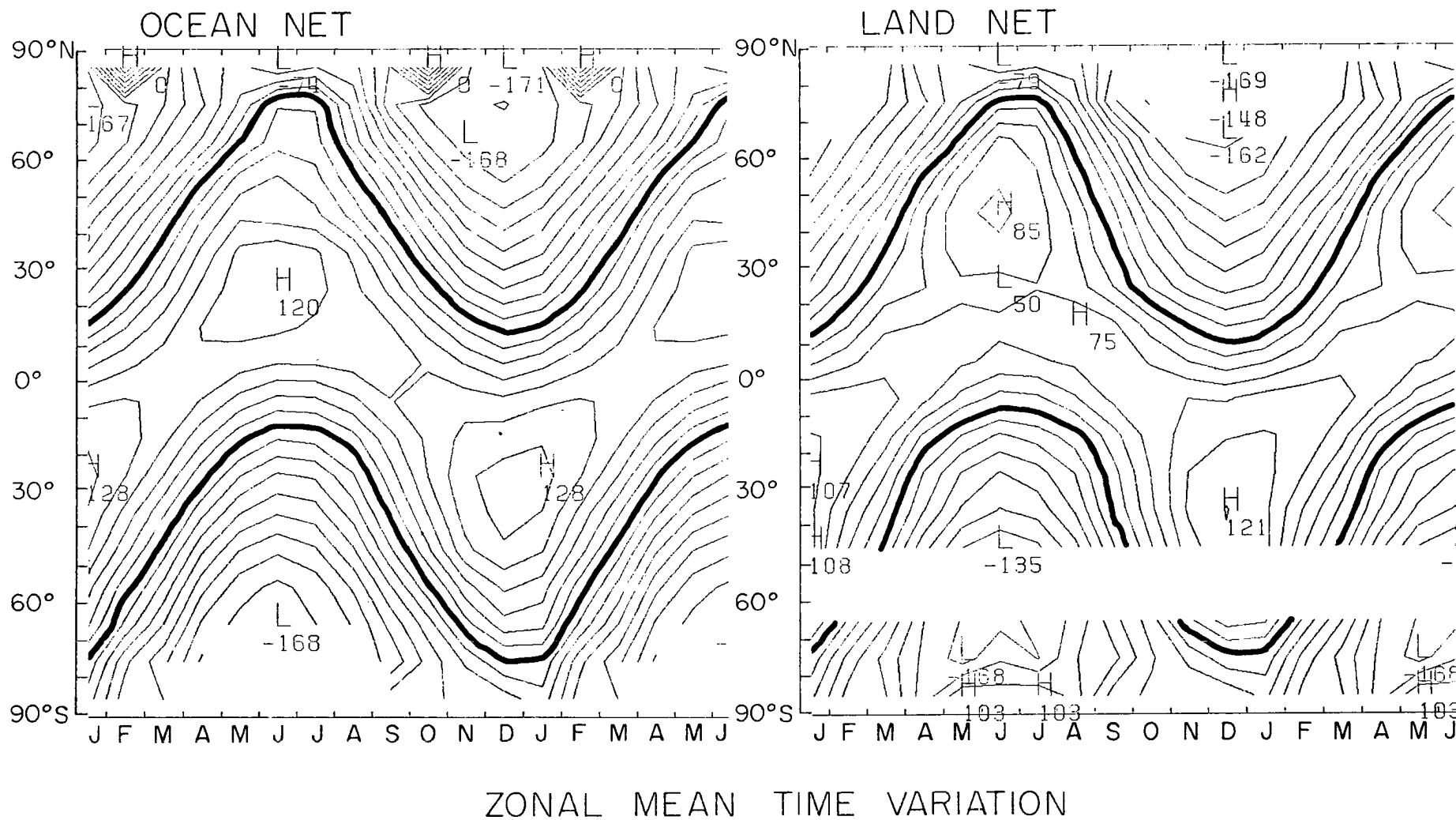


ZONAL MEAN TIME VARIATION

Figures 6b & 7b. Contour Interval 2.5%. Heavy line at 25%.

Figure 6c

Figure 7c



24

Figures 6c & 7c. Contour Interval 20 W/m². Heavy line at 0 W/m².

these zonal plots the need for separate calculations for both land and ocean even in simple zonal average climate models.

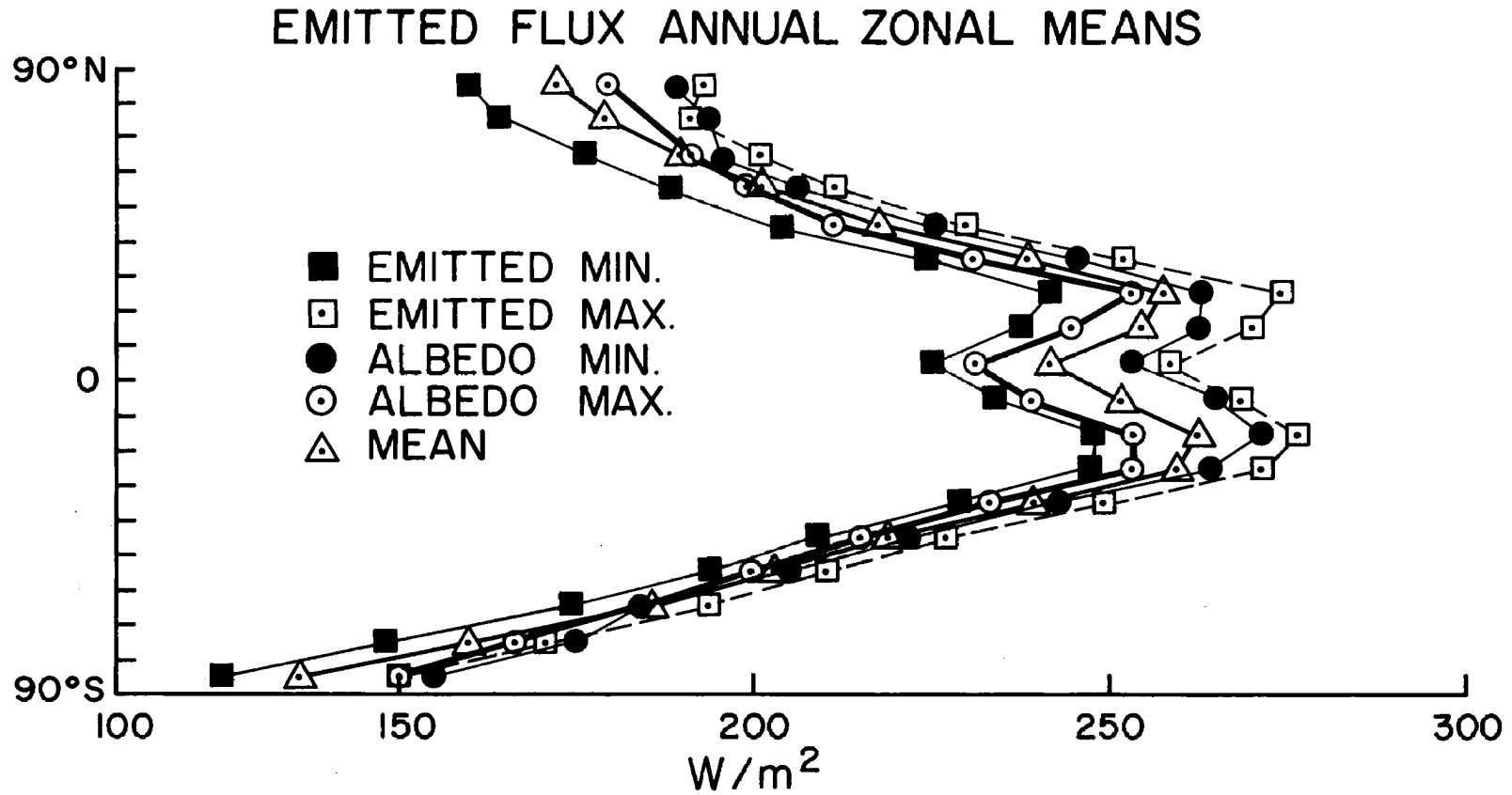
Extremes

As a measure of the possible weather variability we have constructed some annual average extreme maps. First, each individual month map was rescaled to the same 70°N to 70°S area average to remove most of the systematic inter-instrument differences. Most of the remaining variation was due to changes in the average weather for the particular years observed. Each monthly set was searched for the extreme of either albedo or emitted flux then the albedo and emitted was stored for that situation. Finally the annual average was compiled for each of the four possibilities. Fig. 8 shows the zonal averages for the five situations - average, maximum emitted, maximum albedo, minimum emitted, minimum albedo. One sees that there is less variation in the net than might be expected if the covariance of emitted and albedo were not considered. Unfortunately, one cannot be assured that the differences here are not partially caused by systematic errors between sensor systems. Table 5 lists maximum deviations from the mean in the 18 latitude zones. This is the outside limit of variations due to weather events possible, as it is very unlikely that all regions in a particular latitude zone might be shifted from the normal in the same sense.

Relative dispersions

Another measure of the weather variability is the dispersion of the measurements around the mean. Vonder Haar (1972) and Raschke et al. (1973) discussed this concluding that regions with large dispersions were regions where significant climate events could occur. In other

Figure 8a



The annual zonal means of the extreme situations give an indication of the maximum fluctuations possible as seen in the observations. The triangles show the mean of all the data.

Figure 8b

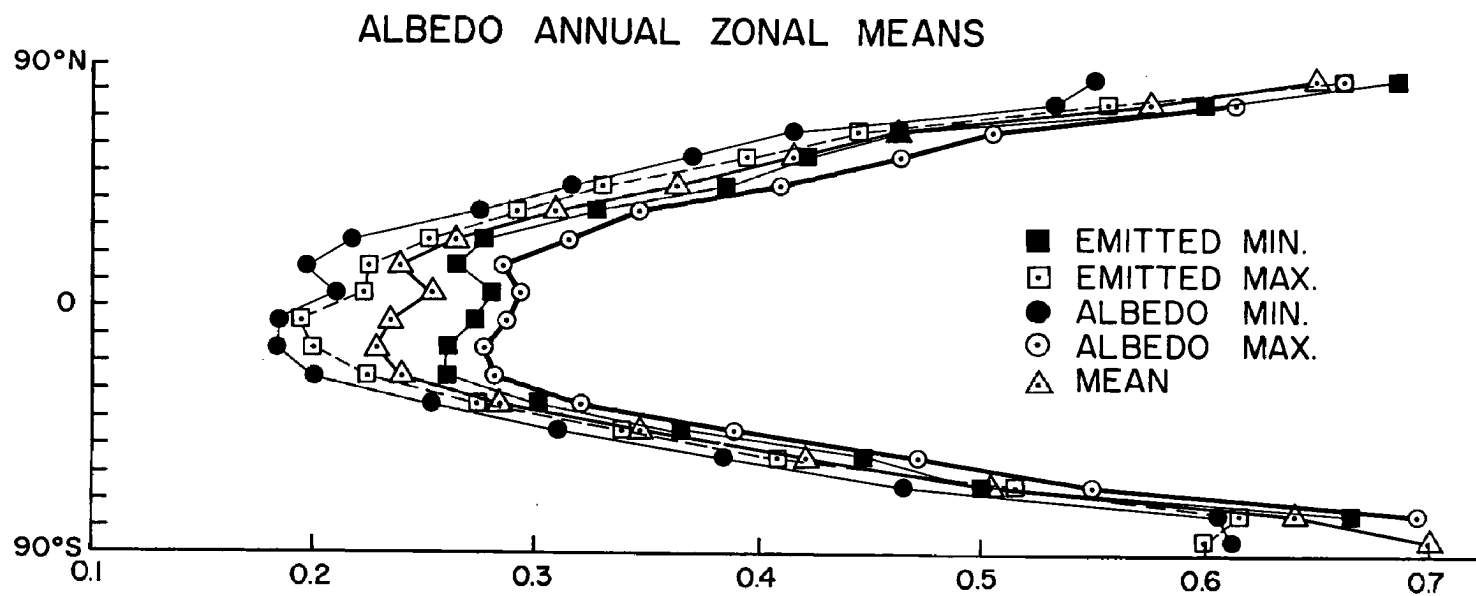


Figure 8c

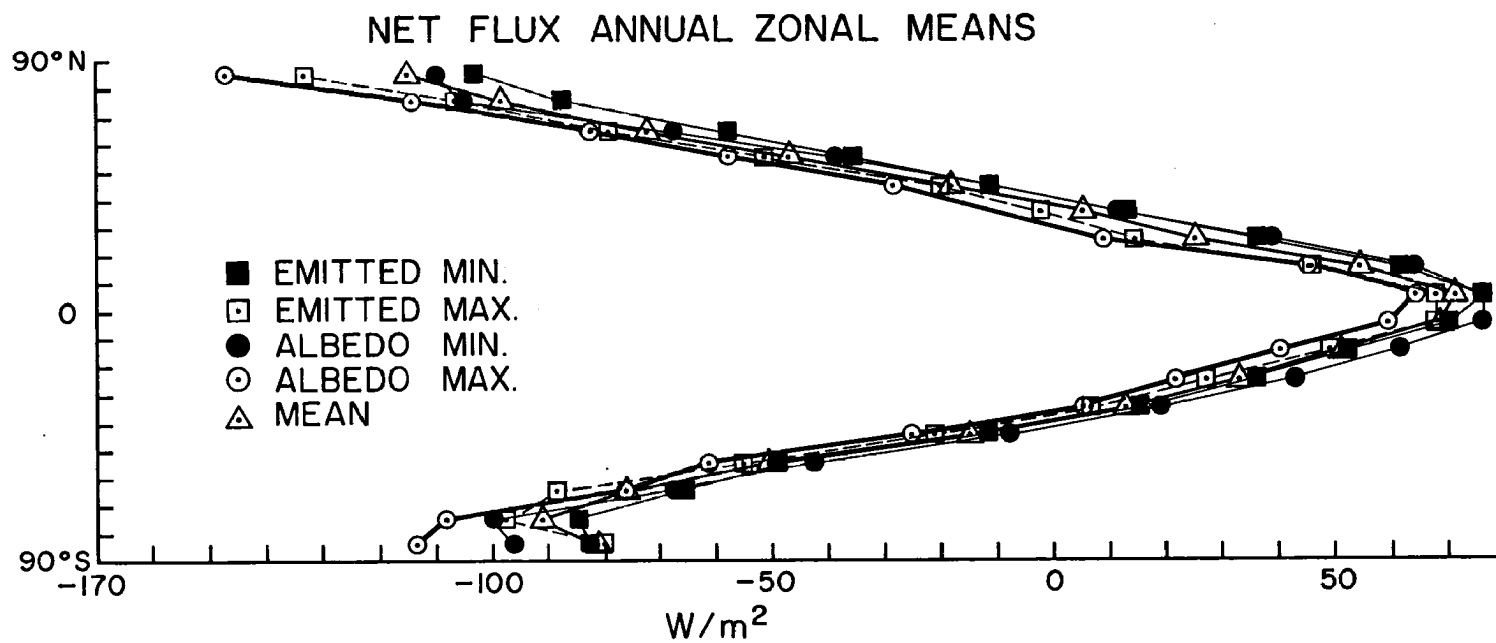


Table 5. Weather Related Variation of Annual Means

	Emitted W/m^2			Albedo			Net W/m^2		
	Min	Av	Max	Min	Av	Max	Min	Av	Max
70-60N	176	191	201	.42	.46	.51	-82	-72	-57
	189	201	212	.37	.41	.46	-58	-46	-35
	204	217	230	.32	.36	.41	-27	-18	-12
	224	239	253	.27	.31	.35	-3	6	14
	242	258	274	.22	.26	.32	10	25	39
	238	254	270	.20	.24	.29	46	55	64
	225	241	258	.21	.25	.30	65	72	77
	234	251	268	.18	.23	.29	59	70	76
	248	262	276	.18	.23	.28	40	52	61
	248	259	271	.20	.24	.28	23	33	43
	229	239	249	.25	.29	.32	5	12	19
	210	218	227	.31	.35	.39	-25	-16	-7
	194	203	211	.38	.42	.47	-61	-60	-43
60-70S	175	185	194	.46	.51	.55	-88	-77	-66

The annual zonal mean of the extreme situations gives an indication of the maximum deviation caused by weather events, see Fig. 8. Av refers to the zonal average of the annual map. Min and Max refer to the annual average of a set of extreme maps for each individual month. Poleward of 70° are not listed because of sparse sampling.

words, events in the atmosphere-ocean system which cause significant changes in the radiation budget are most likely to recur where they have been seen before. Climate modeling and prediction schemes must simulate these regions of high variability better than the regions of low variability.

The variance of each set of monthly observations about the month mean was calculated and then the 12 month average dispersion was determined (Eq. 3).

$$\text{dispersion} = \sqrt{\sum_{m=12} \left[\sum_{\text{obs}} (\chi_n^m - \bar{\chi}^m)^2 / N^m \right]} / 12 \quad (3)$$

$$\chi_n^m = n^{\text{th}} \text{ observation of the } m^{\text{th}} \text{ month}$$

$$\bar{\chi}^m = \text{mean of month } m$$

$$N^m = \text{number of observations in month}$$

As described above, the normalized maps were used to remove inter-satellite differences. Strictly speaking this dispersion is the standard deviation of any particular month from the monthly mean. This small sample size, about 4 observations for any month, make this rather imprecise. The dispersion of reflected exitance rather than albedo is presented because this provides the proper energy weighting.

One can see in the maps (map 14) that large dispersions occur at the edges of large amplitude features in the mean maps. East and west of the monsoon there are regions of high variability in both the reflected and emitted. This is probably produced by different sized monsoons. The central region is persistent in all samples but the fringes change from year to year. The largest variations occur in reflected and emitted over South America and west of South America,

but there are only weak maxima in the net radiation dispersion. These year to year differences show the negative correlation between emitted and reflected, reciprocity, damping out the variation of the net. The biggest dispersion of the net occurs over the large continental deserts, the Sahara, S. Africa and Australia. There the reciprocity does not reduce the net variance. The large dispersion in both the reflected and emitted compliment each other amplifying the net year to year changes. The large dispersion in the North and Central Pacific appear primarily because of changes in the reflected component.

These dispersions can also be interpreted as a measure of the uncertainty of the monthly mean. The standard error of the mean is about one half (four measurements of each month) of the dispersions. The real uncertainties are larger than this though, because of systematic errors.

Monthly Maps

There are 36 monthly mean maps presented with (on some) notes listing some interesting details. The discussion here will be different, picking one feature and following it through time.

The most prominent non-zonal feature is the large monsoon circulation seen around India and South East Asia. One sees a blooming of the albedo over China, South East Asia and India in June. Simultaneously there is a decrease in the exitance. Both are caused by clouds. It is very significant that the net radiation is little changed by the appearance of this large cloud mass. Thus one suspects that unusual monsoon cloudiness patterns would change the albedo and exitance away from the climatology, but it would not change the net. This remains to be proved once variations from the mean can be examined.

There seems to be a north-south movement of the high albedo region over Pan-America and a similar movement over equatorial Africa like the monsoon caused changes in clouds. These two features produce the prominent seasonal cycle in the zonal average land profiles discussed above. These change the net radiation whereas the monsoon did not.

Over the northern hemisphere continents one can see hints of the location of large snow and ice regions and their seasonal change in the albedo maps. Here the poor sensor resolution and the aliasing due to the dark pole make the results uncertain. For future experiments it will be necessary to utilize higher resolution instruments in this region of large discontinuity to monitor the radiation budget and its detailed time changes.

The Sahara desert shows the largest variation in the net because of its large temperature variation. The largest gradients of net radiation occur between the Sahara and the oceans both east and west in the summers. This does not lead immediately to atmospheric energy transport because of the thermal inertia of the ocean. It probably contributes as a source of energy for that energy released into the atmosphere by the monsoon.

Regional Studies

Longitude Sections

We have examined many of the latitude or longitude vs time cross sections and a few are quite interesting. Fig. 9 shows the radiation budget components for 10° - 20° N which is the region with the monsoon. Both the emitted radiant exitance and albedo show very large changes east of the Arabian sea, but the net shows much less variation. In fact, the

Figure 9c

$\Delta = 10 \text{ W/m}^2$

NET CROSS SECTION 10-20°N

W/m^2

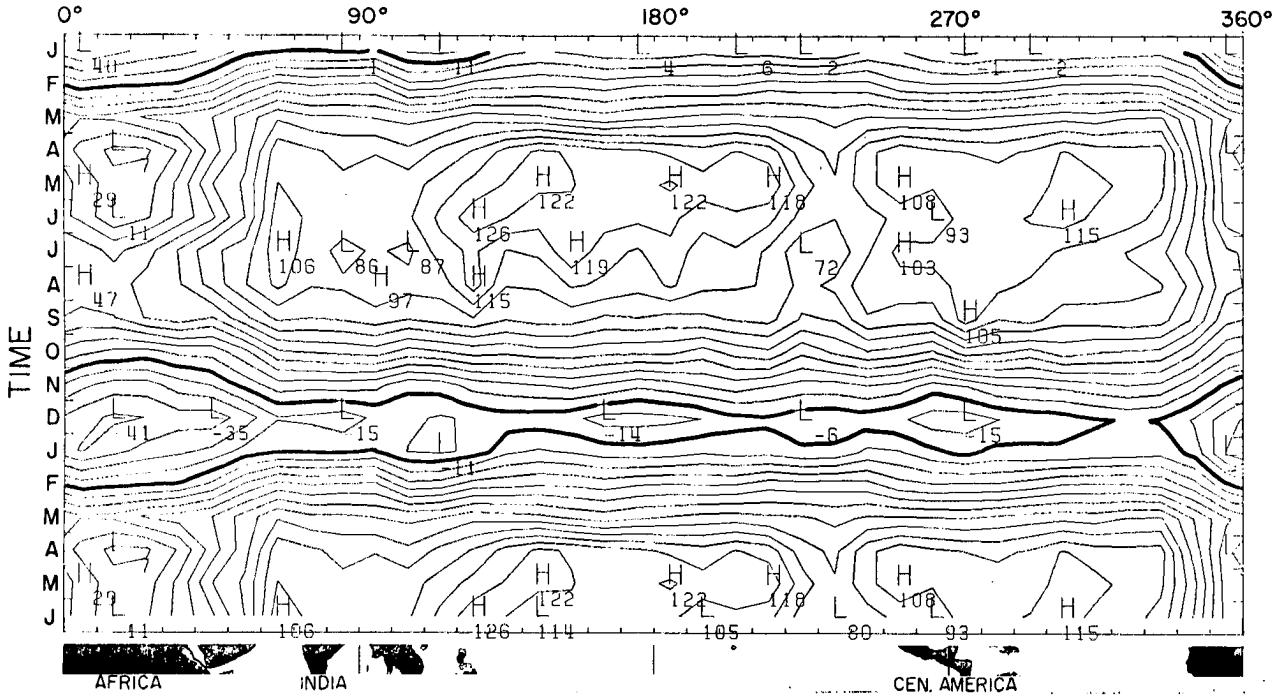


Figure 9d

$\Delta = 10 \text{ W/m}^2$

NET CROSS SECTION 10-20°N

W/m^2

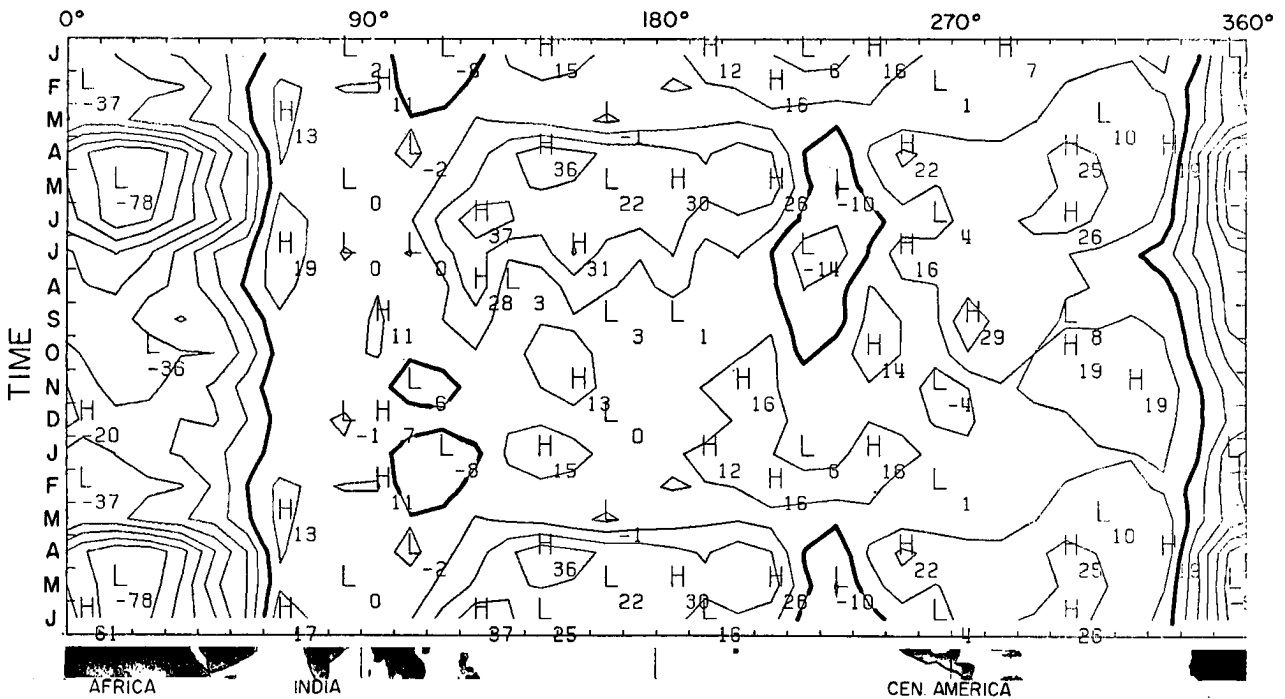


Figure 10c

$\Delta = 10 \text{ W/m}^2$

NET CROSS SECTION 20-30°S

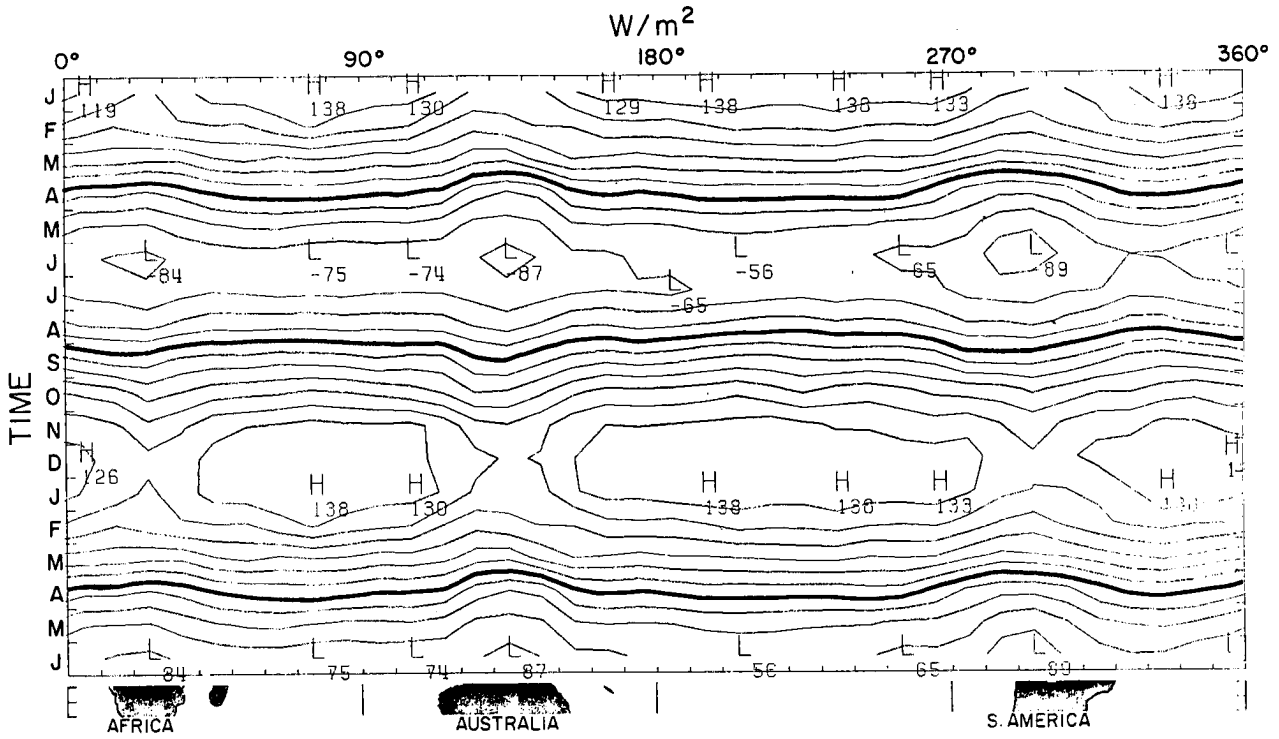
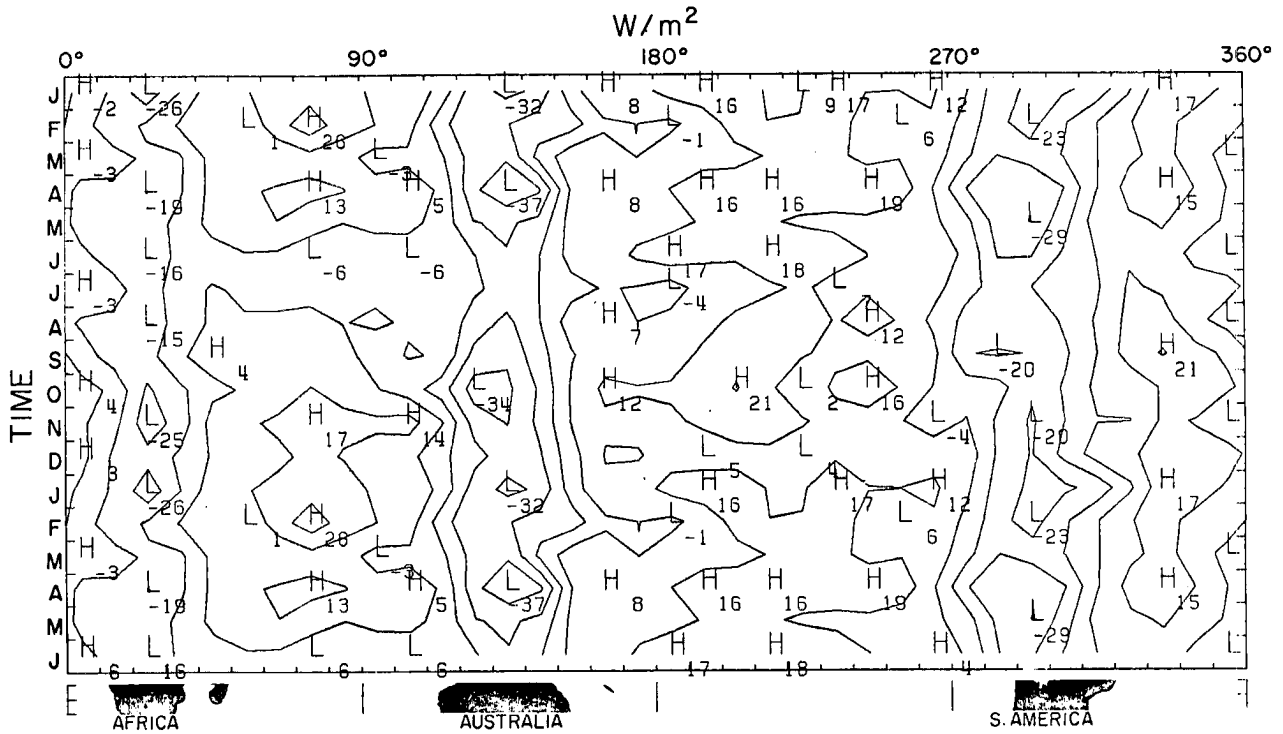


Figure 10d

$\Delta = 10 \text{ W/m}^2$

NET CROSS SECTION 20-30°S



most unusual variation occurs at the southern edge of the Sahara which has the highest emission in April and decreases to a minimum in August as clouds migrate in from the south. These clouds cause an increase in the net over the same situation with no clouds. Fig. 9d shows this as the deviation from zonal mean changes from -72 W/m^2 to -40 W/m^2 from May to August and September. This shows the sensitivity of particular regions to the position of persistent weather features. One suspects that there was a significant abnormality in the cloud field and thus the radiation budget during the recent drought in the sub-Saharan.

The region with the three wave pattern is shown in Figure 10, the latitude section from 20°S to 30°S . The deviation from the zonal mean, net map shows the three lowered regions over Africa, Australia and South America. The low net region around South America and Africa extends to the West because of the low stratus clouds in this region. This is exemplified by the expanded high albedo region (above 25%) in July, August and September in these two regions.

Particular Regions

To segregate even finer regions we have taken small area averages. This is the limit of the resolution of the observations and sharp discontinuities will have been smoothed out. About 50 regions with approximately uniform climatology were examined. Several predictable effects are seen in the regions. Fig. 11 shows a typical mid-latitude ocean area with a small seasonal change in emitted flux following the temperature. The albedo shows the expected variation with sun angle. The net flux is surprisingly featureless, depending primarily on the incident flux. Only a few regions showed time variations different than this simple seasonal oscillation.

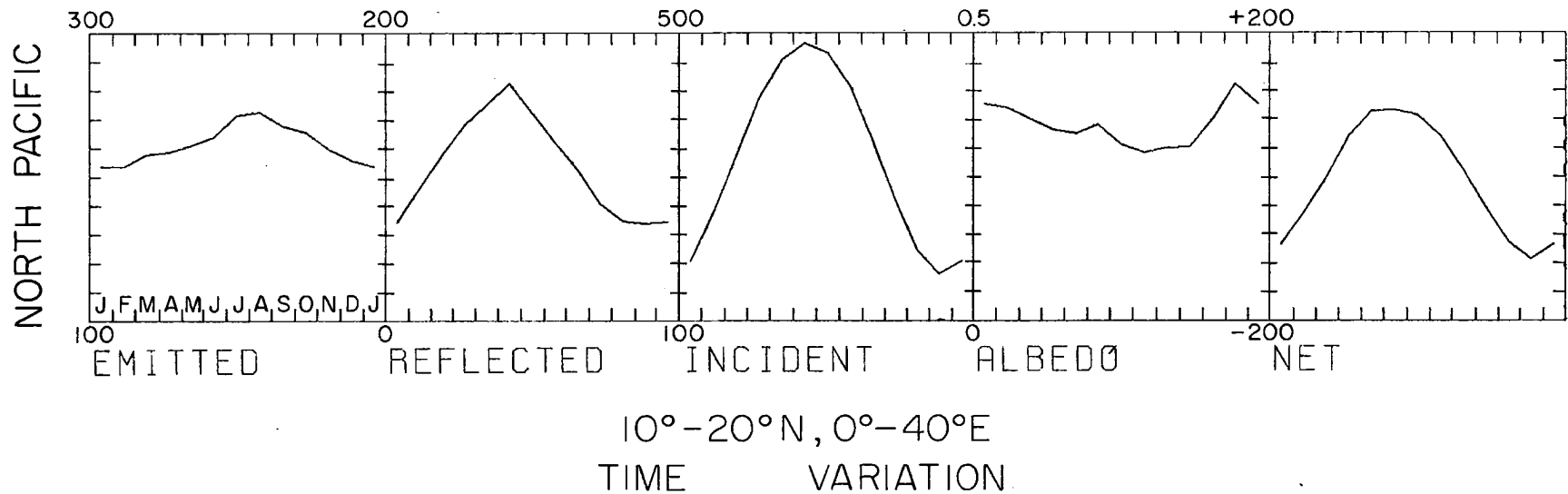


Figure 11

The time variation of the parameters for a typical region. Notice that the albedo decreases as the sun angles increase. The emitted flux increases from winter to summer. The net follows the shape of the incident.

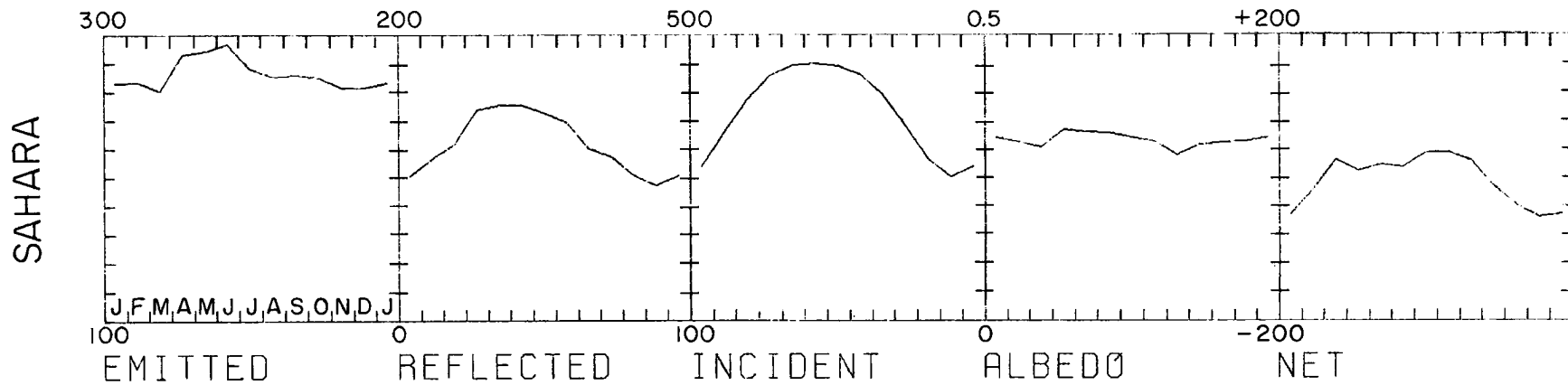
The most varied regions lie between the Sahara and South East Asia. In the desert regions, high temperatures change the exitance enough so that the net flux is perturbed from its normal seasonal change (Fig. 12). The region just south of the Sahara seems to show the migration of clouds in and out of the region during the summer (Fig. 13, as mentioned above).

The appearance of large amounts of clouds is obvious in the plots of the monsoon regions, (Fig. 14). The reciprocity between cloud albedo increases and decreases in exitance are nearly perfect in these regions. To determine the reciprocity more quantitatively one would like to examine year to year differences but this must await a longer time series with more consistent data. We looked through all the regional plots over the globe looking specifically for areas in which cloud changes seemed to change the net and the south Sahara region was the only clear cut example. Probably smaller regions show variations in the net because of particular cloud types and also because of substantial year to year changes. One must conclude that seasonal changes in cloudiness through the year affects the net very little over most of the globe. Variations around the mean annual cycle may cause more substantive changes.

Conclusions

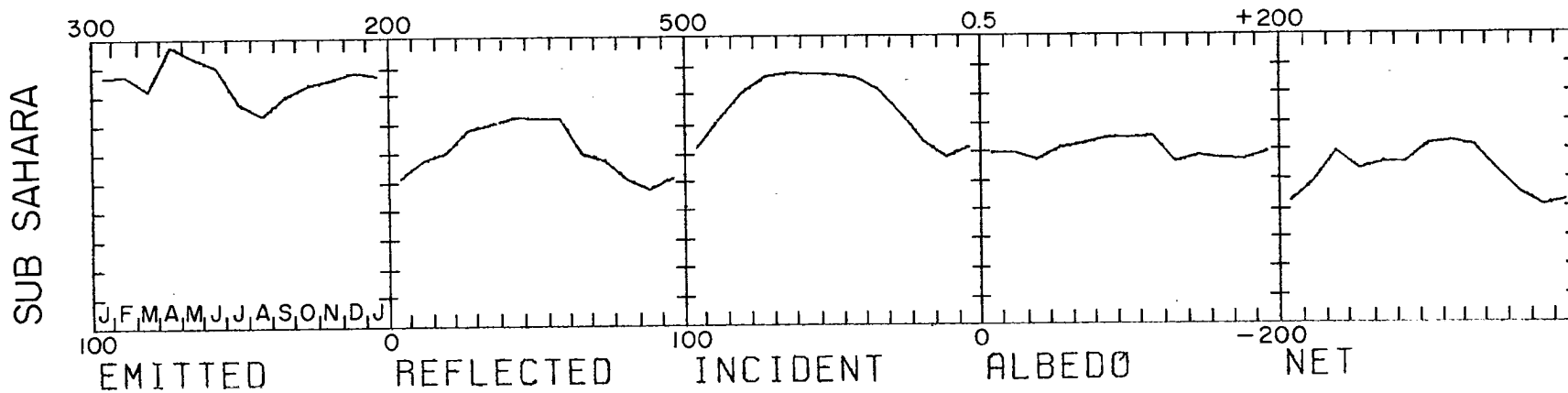
One finds, as is well known, that the sun position is the prime determinant of the radiation budget. The next most important feature is the difference between land and ocean. It is apparent that even the crudest zonal average climate model must take this into account. Clouds have a large effect on the net over land areas (at least in the tropics). Whereas large cloud systems have little effect on the net over the oceans. The oceanic stratus clouds have an effect because of their

Figure 12



10°W-40°E, 10°-30°N
TIME VARIATION

Figure 13



10°-20°N, 0°-40°E
TIME VARIATION

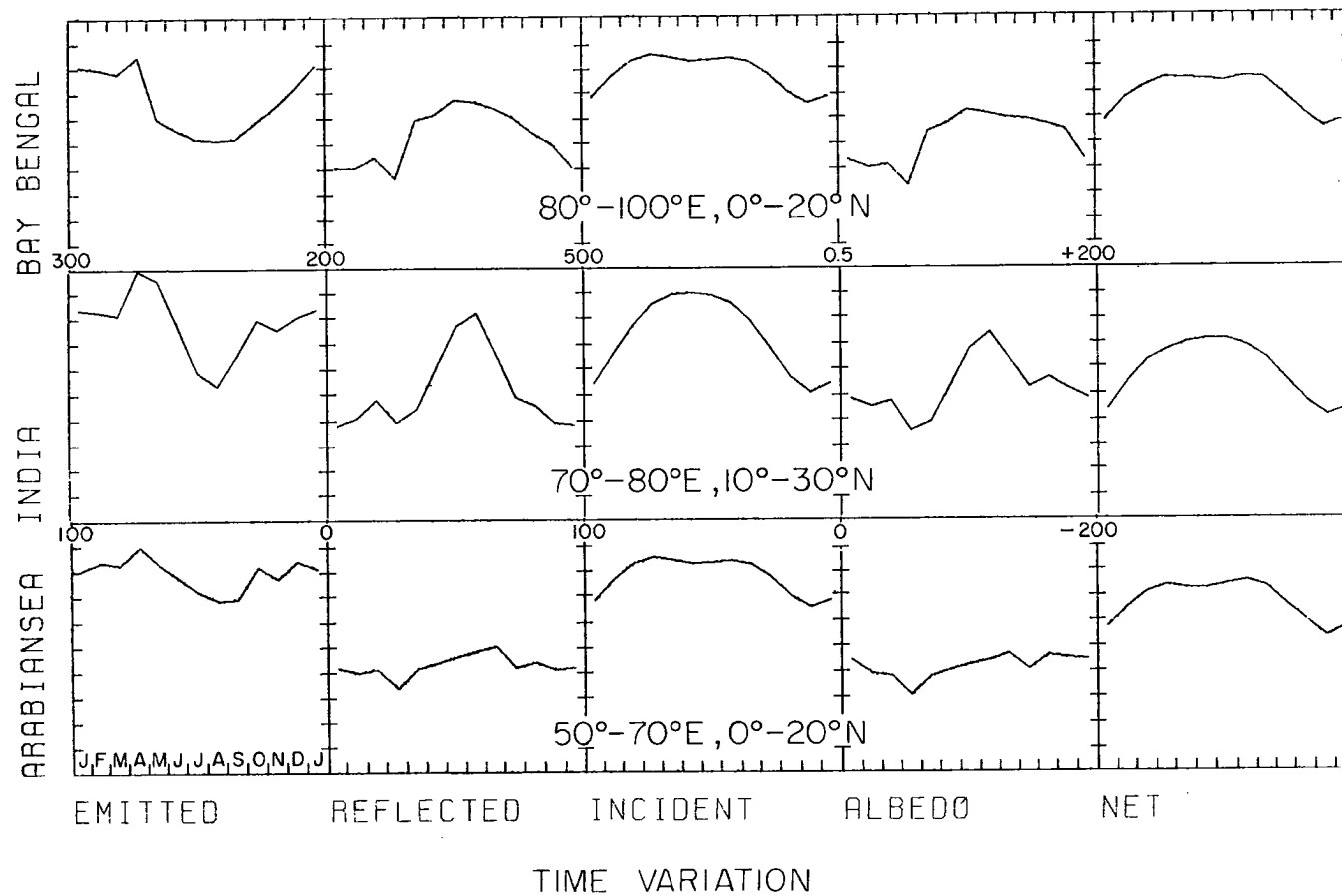


Figure 14

The time variation of these three regions shows the dramatic influence of the Monsoon on the albedo and emitted flux. Reciprocity between these two is shown by the insensitivity of the net to the Monsoon cloud change.

alteration of albedo but not the emitted flux. Thus cloud type as well as amount are both critical parameters for climate modelling.

Large scale circulation patterns are evident in the data but the detection of minor changes would be difficult at this resolution. For instance, a sharp snow line can not be detected in this data. Shifts in the cloud masses over equatorial Africa or South America could have a large impact on the global radiation budget and are detected in this data with 10^0 resolution but just at the resolution limit.

Additional data will improve the accuracy of the monthly mean climatologies. But high absolute accuracy will be needed to improve the accuracy of the annual mean. Systematic errors are the largest source of error in the annual means. One would like to measure the variance due to weather events but we are just on the threshold of being able to do that. The Nimbus 6 and 7 experiments do not have substantially more absolute accuracy but at least they overlap in time. This will allow intercomparisons of their calibrations and measurements and thus inter-annual variation estimates from 1975 and later in future studies.

We will make this data set available to other users on computer tape on request. Large tabulations of the numbers have not been included in this report for that reason.

Credits

We would like to thank Dr.'s H. Jacobowitz and W. Smith of NOAA who supplied the Nimbus 6 observations and Dr. J. Ellis for compiling the many older data sets. Dr. G. Stephens provided several suggestions. L. Parkinson provided invaluable service in typing the many drafts, M. Howes prepared many of the figures and J. Gailiun reviewed the manuscript.

This was prepared under the Nimbus 7 Earth Radiation Budget Experiment of NASA (Contract NAS 5-22959).

References

- Arking, A. and G. G. Campbell, 1980: Effect of directional reflectance on radiation budget measurements at particular local times. In preparation.
- Campbell, G. G. and T. H. Vonder Haar, 1980: An analysis of two years of Nimbus 6 radiation budget measurements. Atmospheric Science Paper #320, Colorado State University, Ft. Collins, CO.
- Crutcher, H. L. and J. M. Meserve, 1970: Selected level heights, temperatures and dew for the Northern Hemisphere, NAVAIR 50-1C-52, revised Chief Nav. Op., Washington, D.C.
- Dines, W. H., 1917: Heat Balance of the Atmosphere, Quart. J. R. Met. Soc.
- Ellis, J., T. H. Vonder Haar, S. Levitus and A. H. Oort, 1978: The Annual Variation in the Global Heat Balance of the Earth, Journal of Geophysical Research, Vol. 83, #C4.
- Ellis, J. and T. H. Vonder Haar, 1976: Zonal Average Earth Radiation Budget Measurements from Satellites for Climate Studies. Atmospheric Science Paper #240, Colorado State University, Ft. Collins, CO.
- Gruber, A., 1977: Determination of the Earth-Atmosphere Radiation Budget from NOAA Satellite Data. Meteorological Satellite Laboratory, NOAA.
- Hickey, J., L. Stowe, H. Jacobowitz, P. Pelegriano, R. Maschhoff, A. Arking, F. House, A. Ingersoll, T. Vonder Haar, 1980: Initial Solar Irradiance Determination from Nimbus 7 Cavity Radiometer Measurements, submitted to Science.
- Jacobowitz, H., W. L. Smith, H. B. Howell, F. W. Nagle and J. R. Hickey, 1979: The first 18 months of planetary radiation budget measurements from the Nimbus 6 ERB experiment, J. Atmos. Sci., 501-507.
- Jenne, R. L., H. L. Crutcher, H. van Loon, J. J. Taljaard, 1974: A Selected Climatology of the Southern Hemisphere: Computer Methods and Data Availability, NCAR Tech. Note/STR-92.
- London, J., 1957: A study of the atmospheric heat balance. Final Report, Contract No. AF19(122)-165, College of Engineering Res. Div., New York Univ., 99 pp. (NTIS NO: PB115626).

- MacDonald, T. H., 1970: Data reduction processes for spinning flat plate satellite-borne radiometers, ESSA Tech. Report NESC 52.
- Raschke, E. and W. R. Bandeen, 1970: The radiation balance of the planet earth from radiation measurements of the satellite Nimbus II. J. Appl. Meteor., 9, 215-238.
- Simpson, G. C., 1927: Some Studies in Terrestrial Radiation. Memoirs of the Royal Met. Soc., Vol. II, #16.
- Smith, W. L., D. T. Hilleary, H. B. Howell, H. Jacobowitz, J. R. Hickey and A. J. Drummond, 1977: Nimbus-6 Earth Radiation Budget Experiment, Appl. Opt., 16, 306-318.
- Stephens, G., G. G. Campbell and T. H. Vonder Haar, 1980: Earth Radiation Budget Measurements from Satellites and their Interpretation for Climate Modeling and Studies, submitted to Journal of Geophysical Research.
- Vonder Haar, T. H., 1972: Natural variation of the radiation budget of the earth-atmosphere system as measured from satellites. Conference on Atmospheric Radiation, AMS, Ft. Collins, CO.
- Vonder Haar, T. H. and J. S. Ellis, 1974: Atlas of Radiation Budget Measurements from Satellites (1962-1970). Atmospheric Science Paper #231, Colorado State University, Ft. Collins, CO.
- Vonder Haar, T. H. and V. Suomi, 1971: Measurements of the Earth's Radiation Budget from Satellites During a Five-year Period. Part I: Extended Time and Space Means, J. Atmos. Sci., Vol. 28, p. 305.
- Vonder Haar, T. H. and V. Suomi, 1969: Satellite Observations of the Earth's Radiation Budget, Science, Vol. 163, p. 667.
- Winston, J., A. Gruber, T. Gray, M. Varnadore, C. Earnest, and L. Mannello, 1979: The Earth Radiation Budget Analysis Derived from NOAA Satellite Data, June 1974 to February 1978. Vol. I and II, Meteorological Satellite Laboratory, Washington, D.C.
- _____, 1978: Earth Radiation Budget Science 1978, NASA Conference 2100.

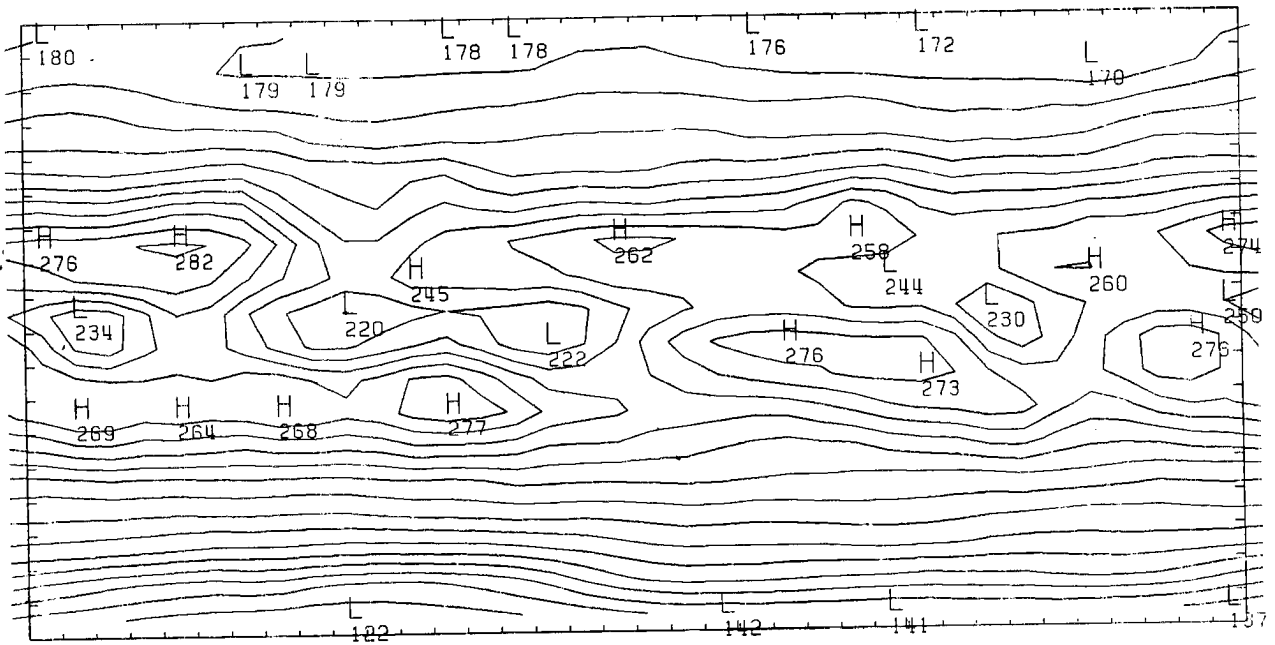
Note on the Maps

All the maps are duplicates of computer plots of 36 by 18 grid point arrays. The data values represent the 10° by 10° area average with the data plotted at the center point of the square. The tick marks around the edge represent the boundaries of the squares. The extension of the lines off the right and left edges represent a circular extension of the field connecting the right and left edges. This is not included on all maps because of an improvement in the computer program during the course of the work. The highs and lows occur at the vertex of the L and at the end of the lower left leg of the H in a cylindrical equidistant projection.

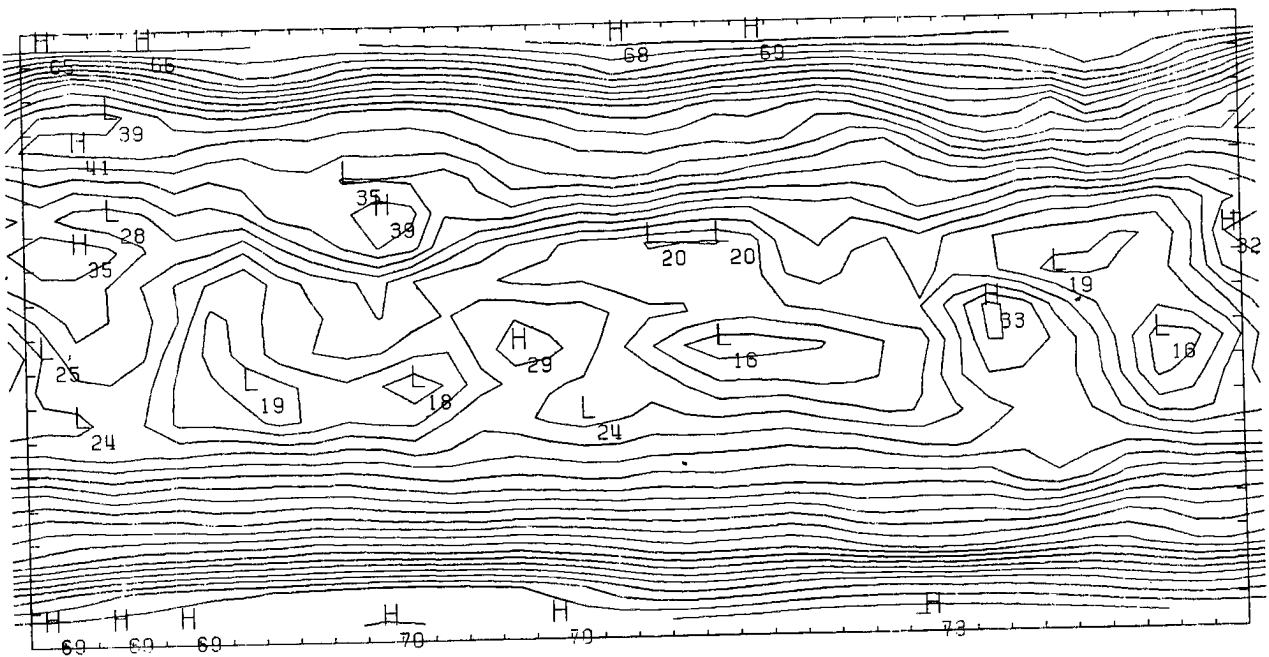
The transparency included is a geographic map in the same projection as the maps and we suggest that it be overlaid on a plot when examining some detail.

The contour interval on all the emitted flux maps is 10 W/m^2 and the contour interval on the net flux is 20 W/m^2 . For all but the annual albedo map a 5% contour interval was used with 2.5% on the annual map.

Emitted

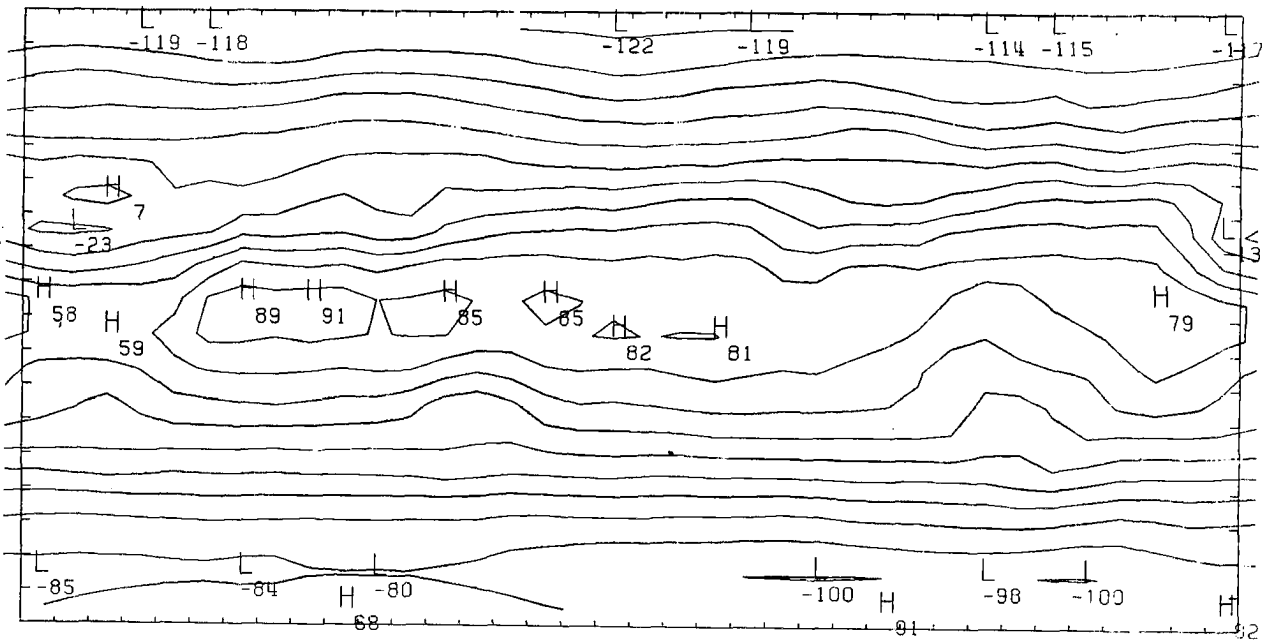


Albedo

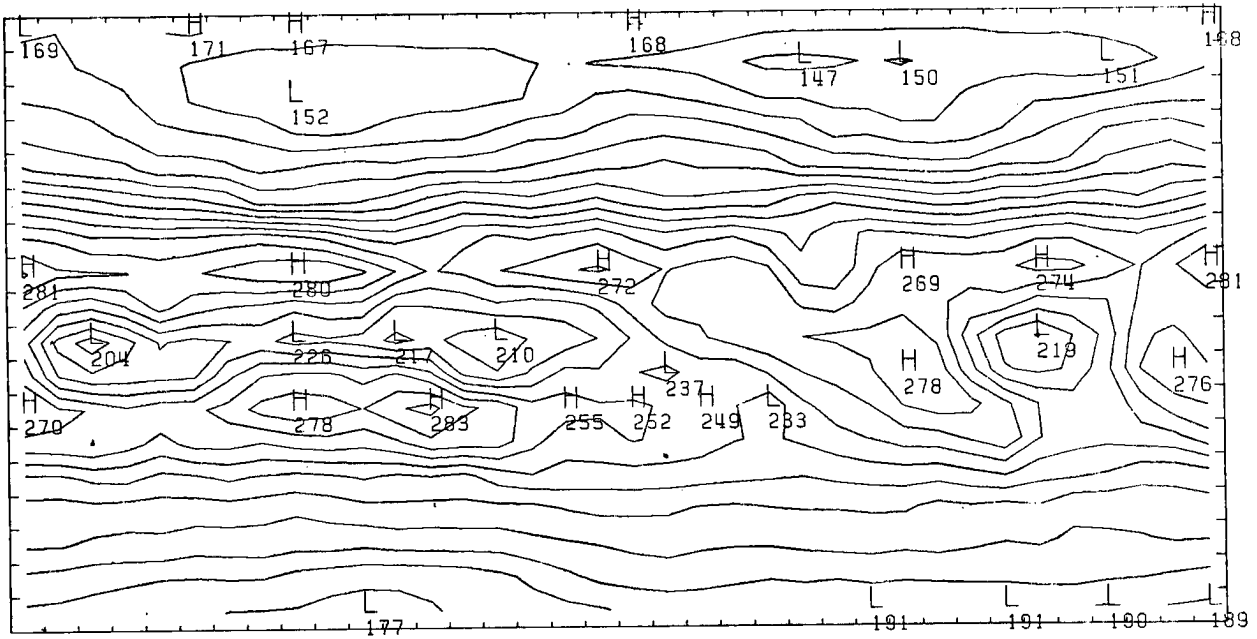


Map #1 Annual

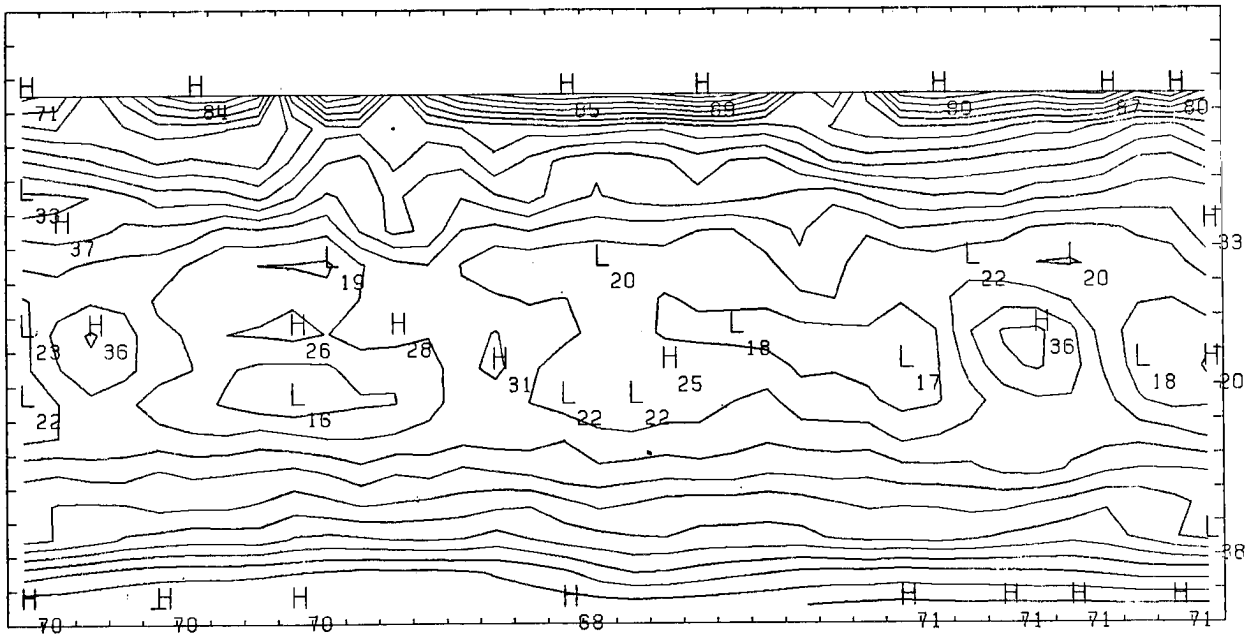
Net



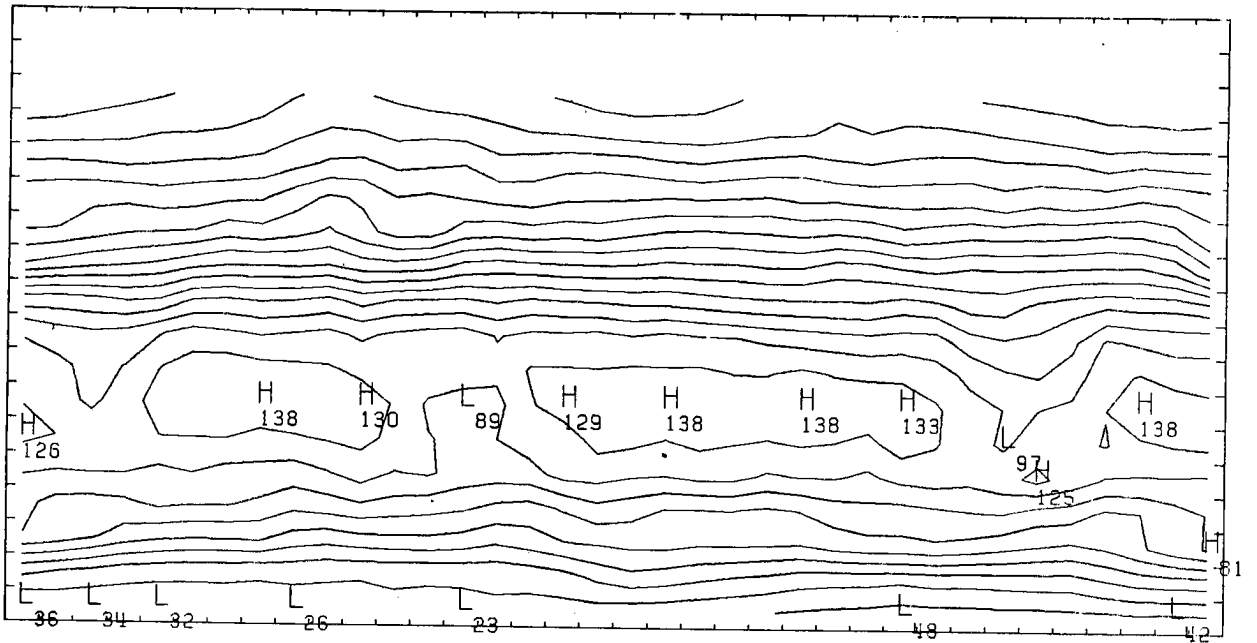
Emitted



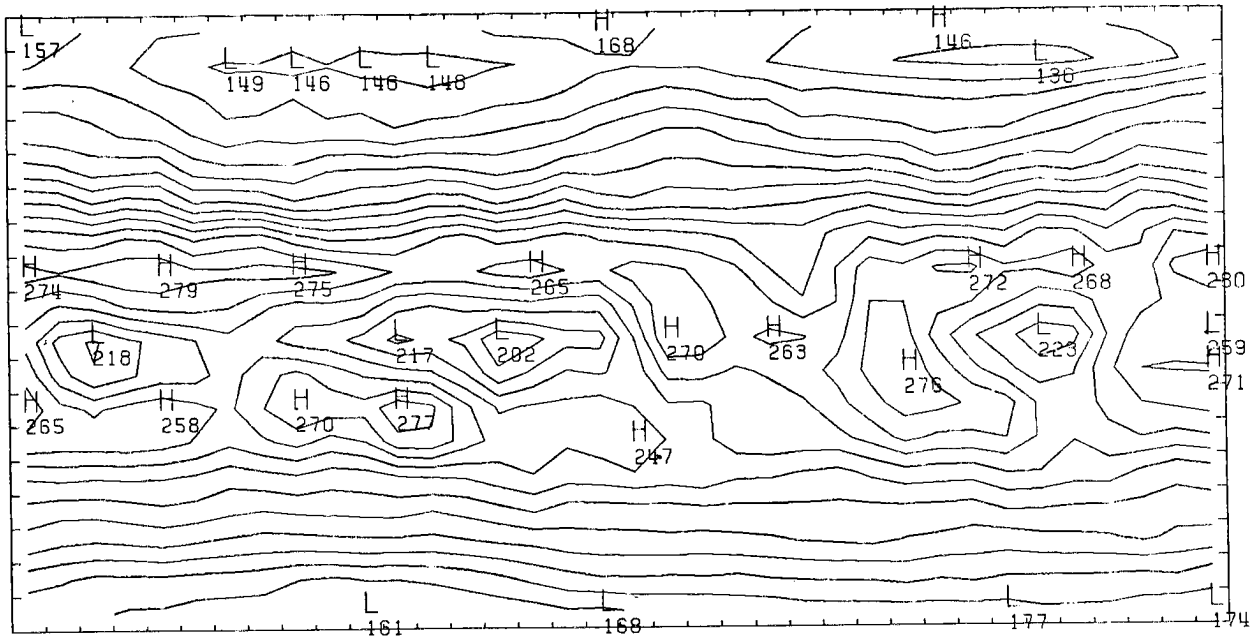
Albedo



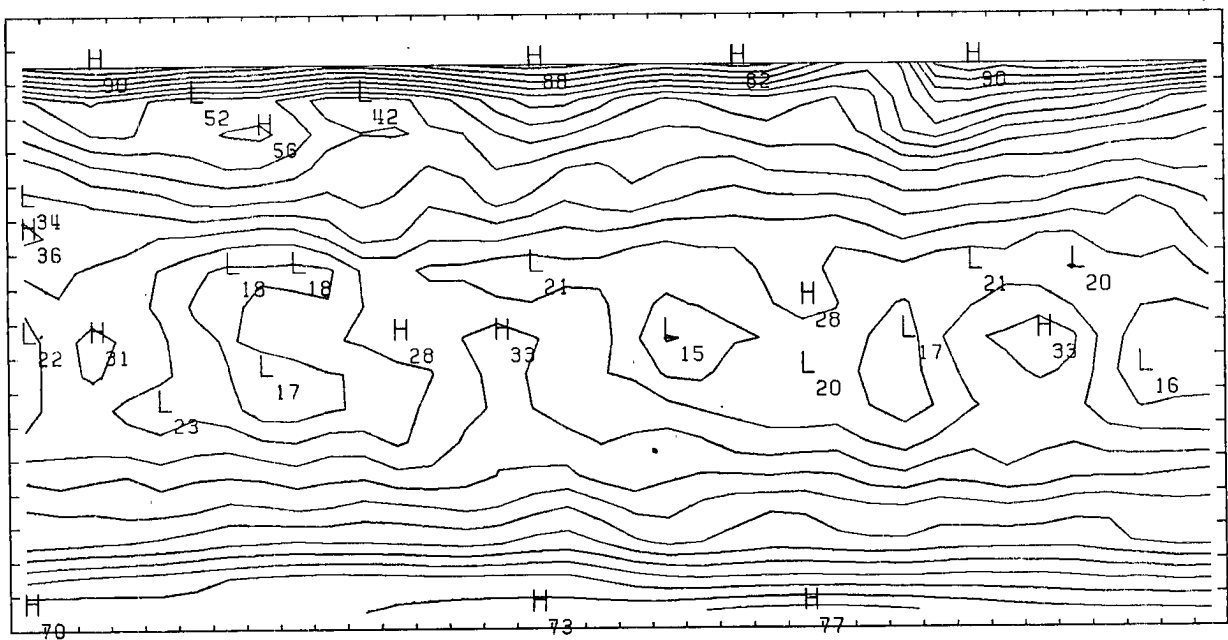
Net



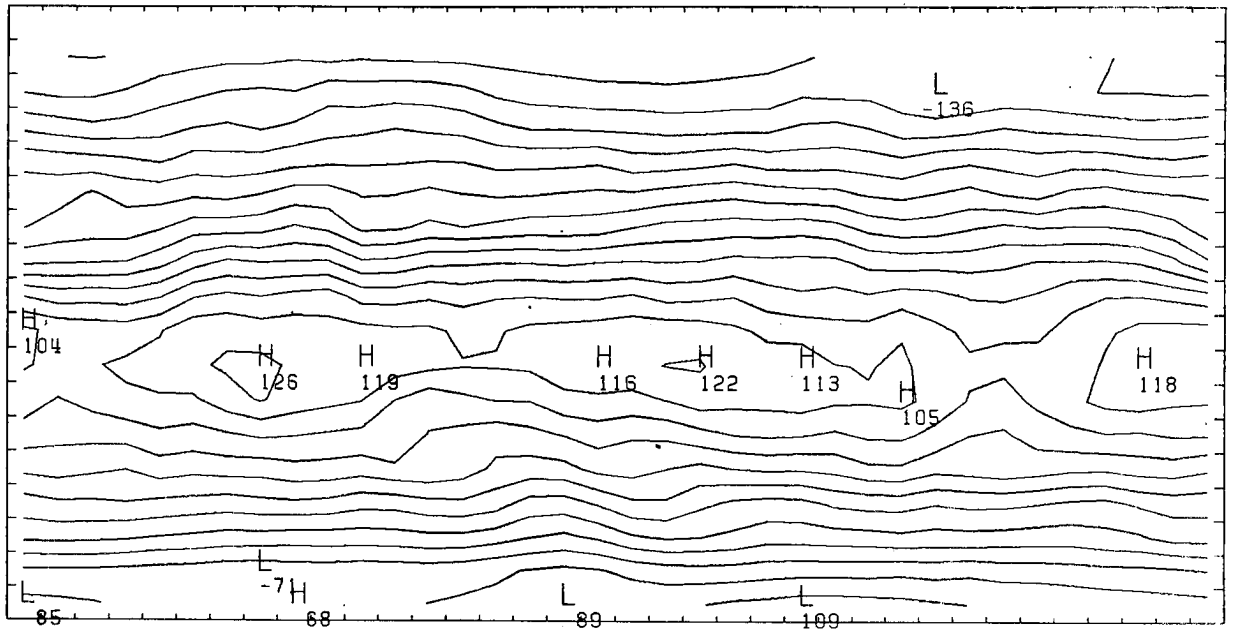
Emitted



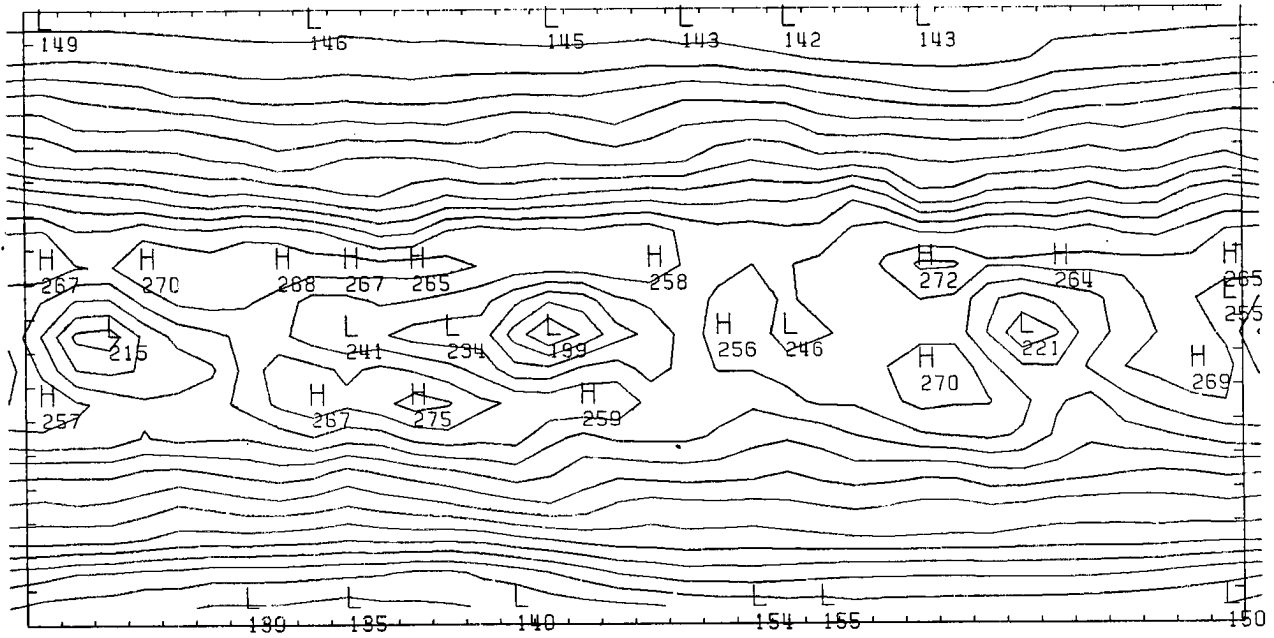
Albedo



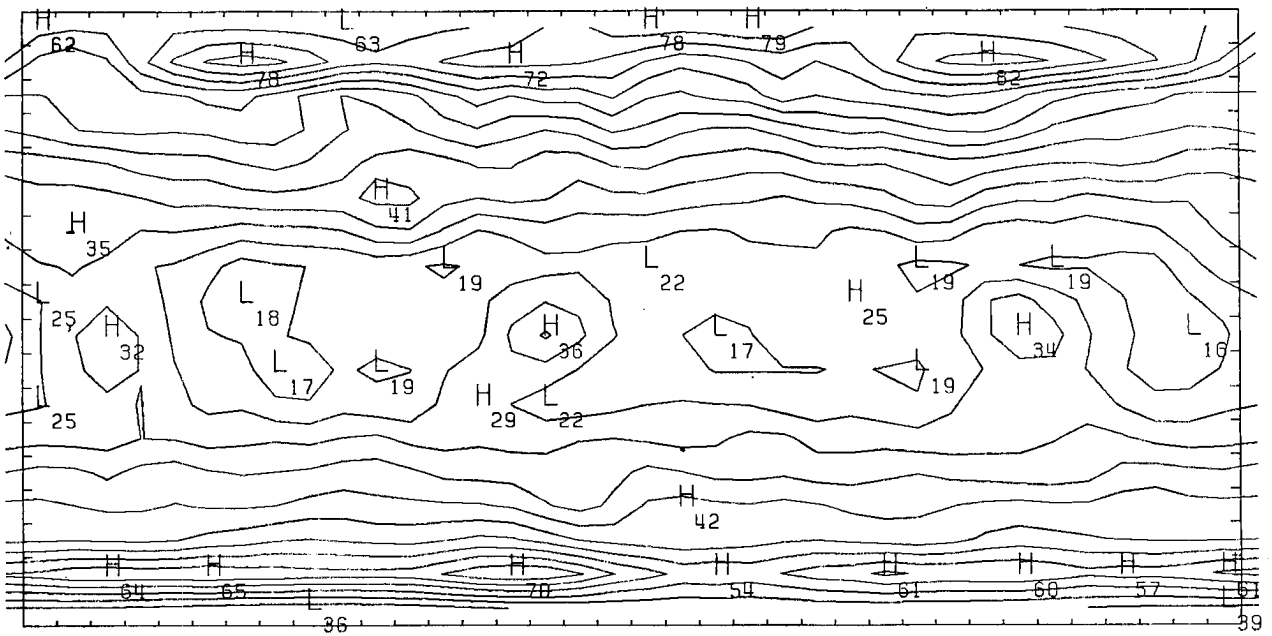
Net



Emitted

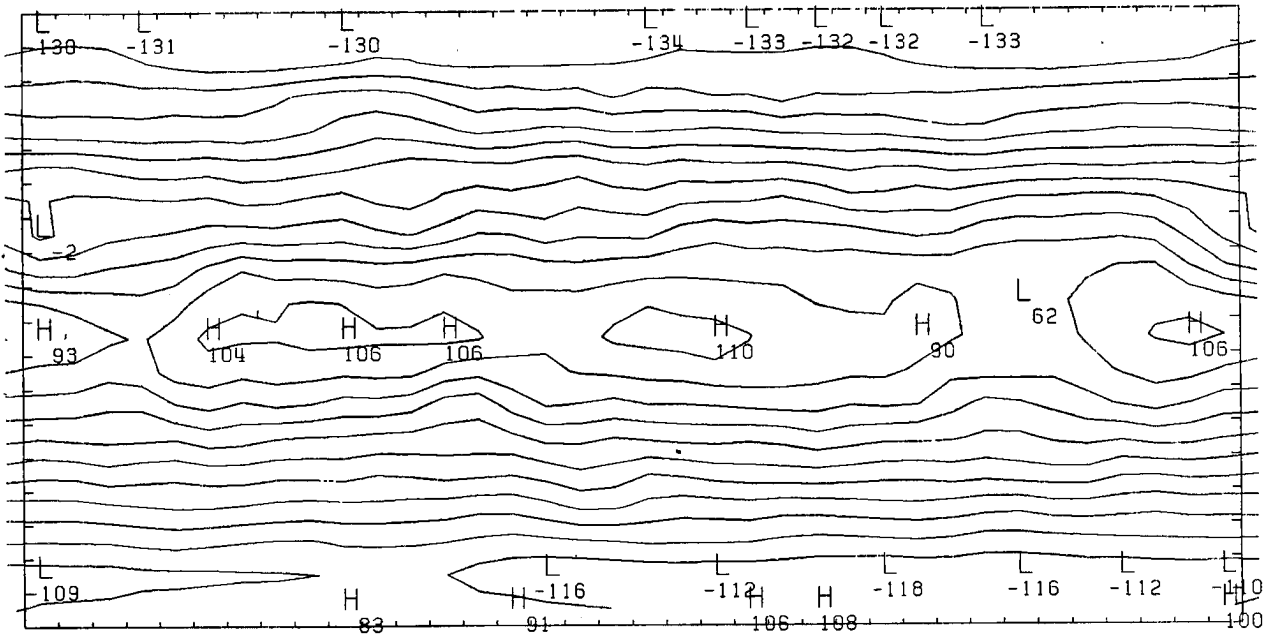


Albedo

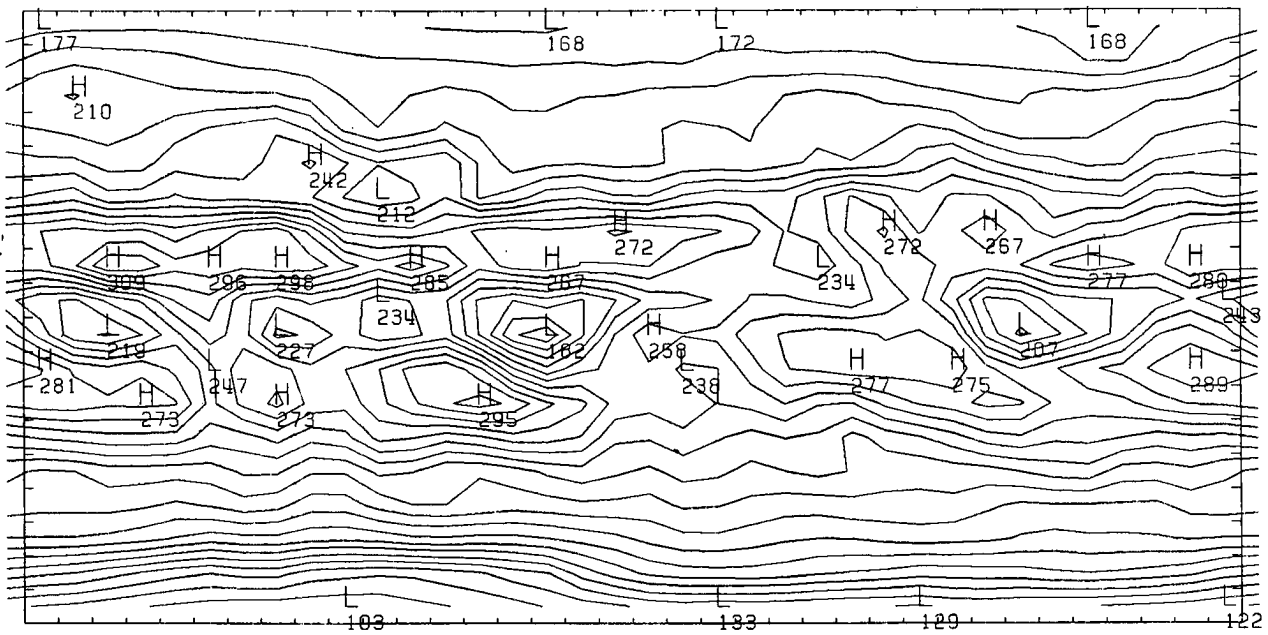


Map #4 March

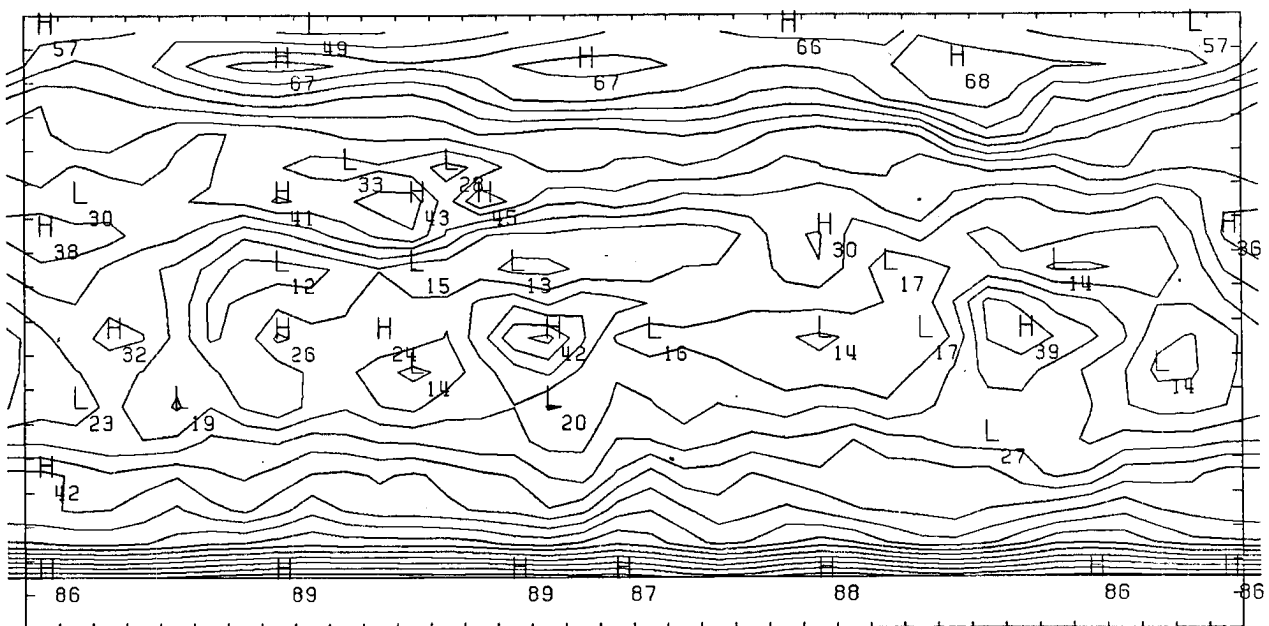
Net



Emitted

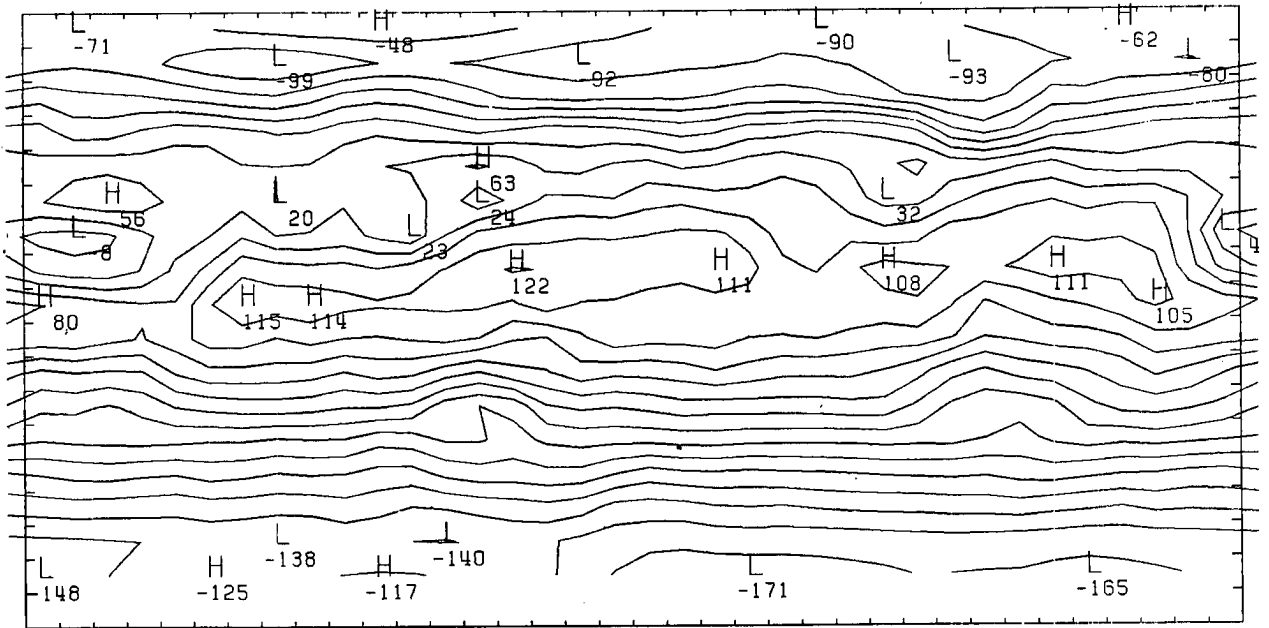


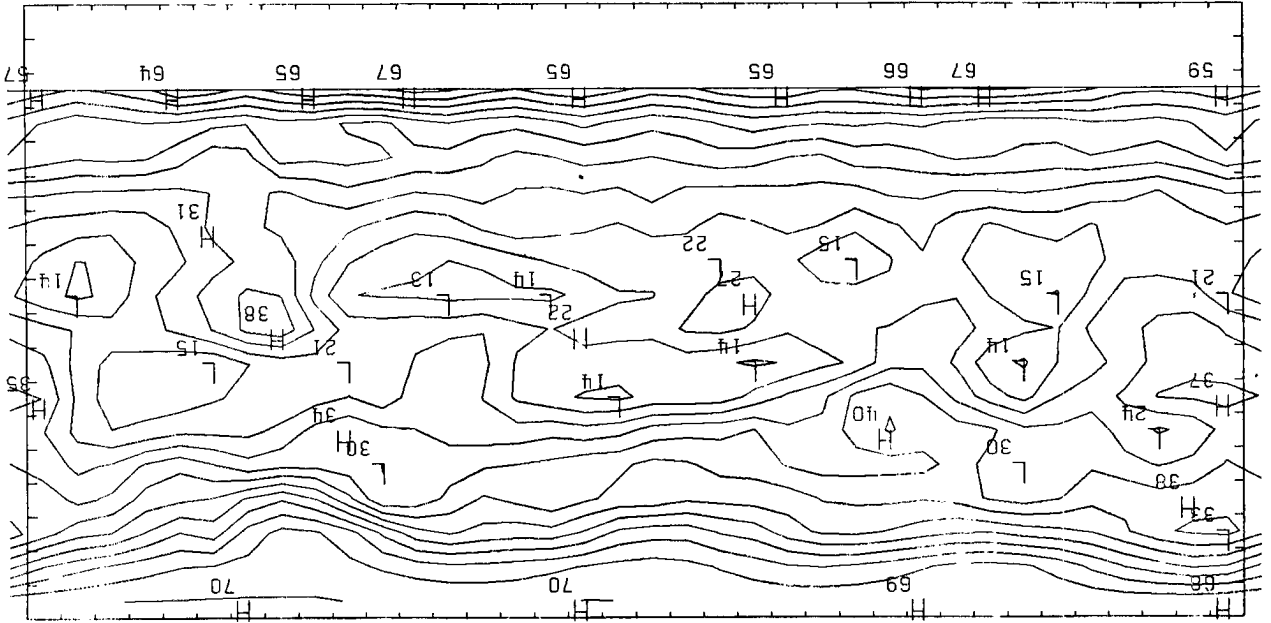
Albedo



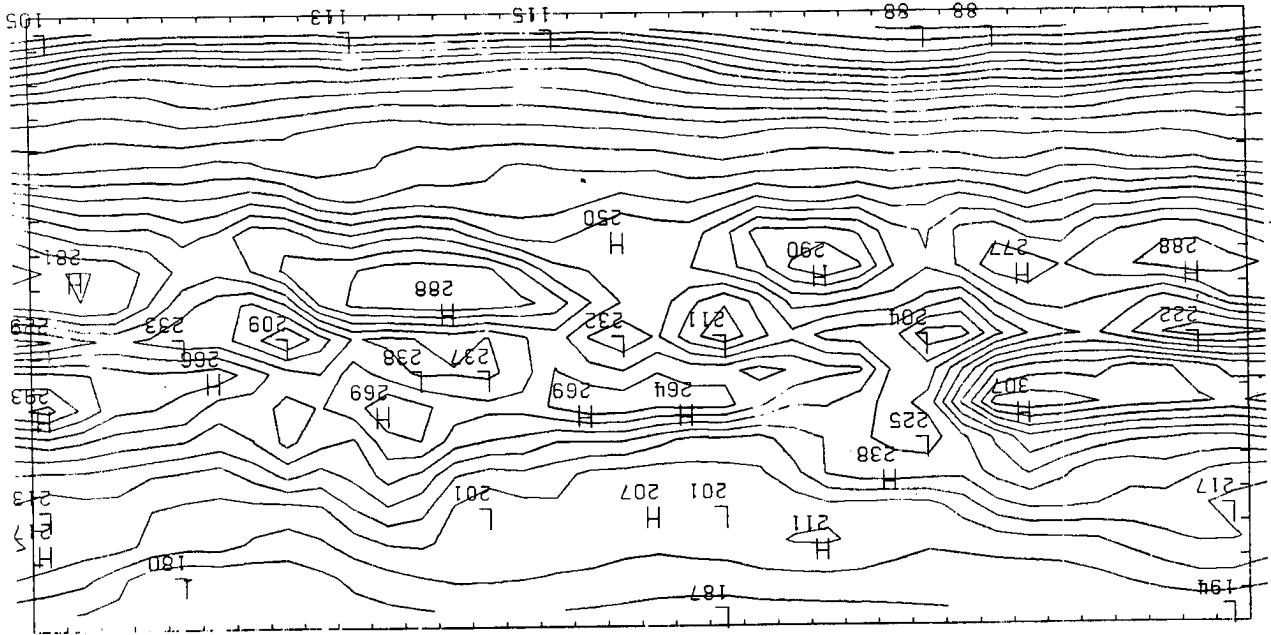
Map #5 April

Net



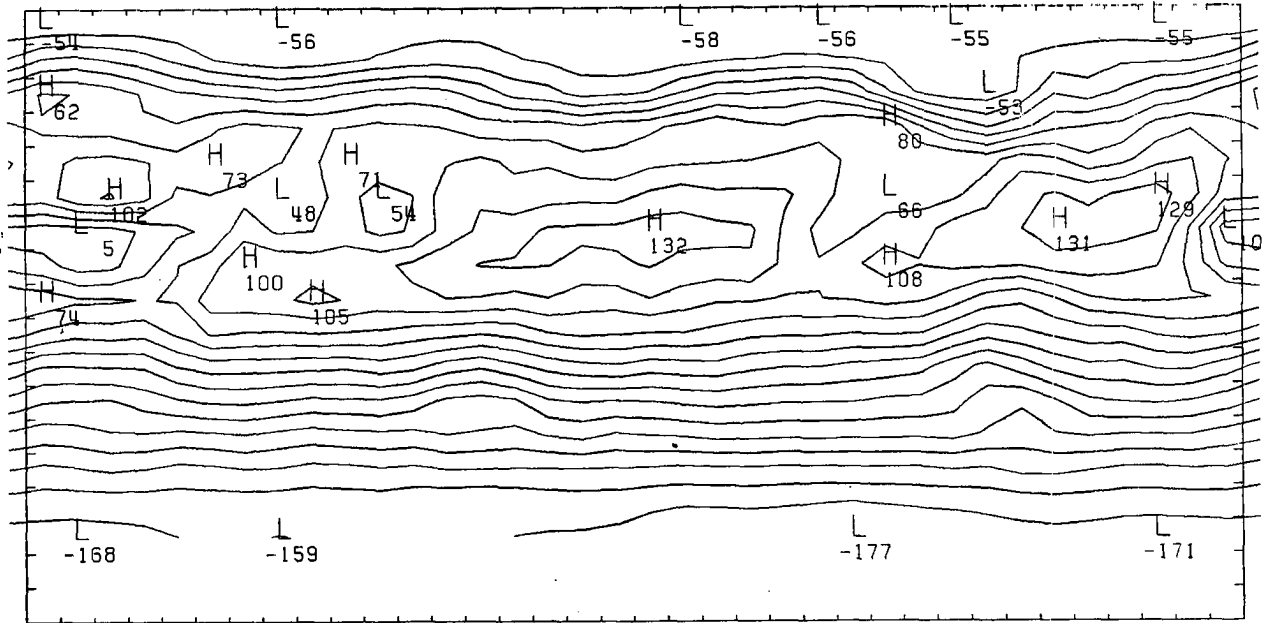


Albedo

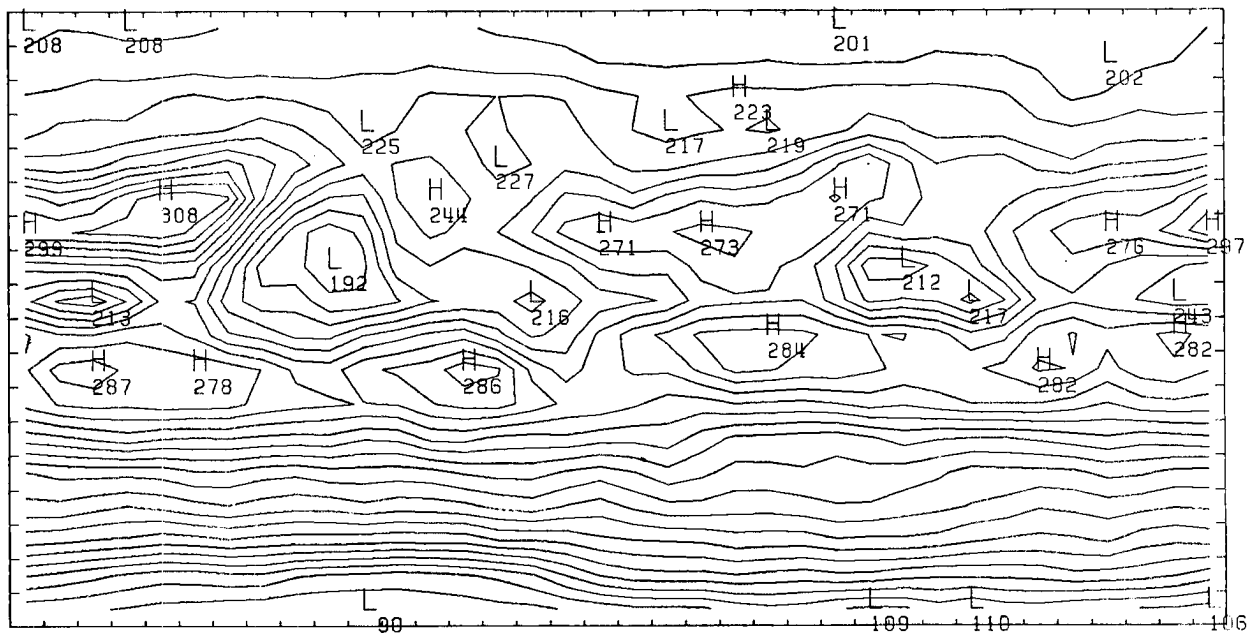


Emtied

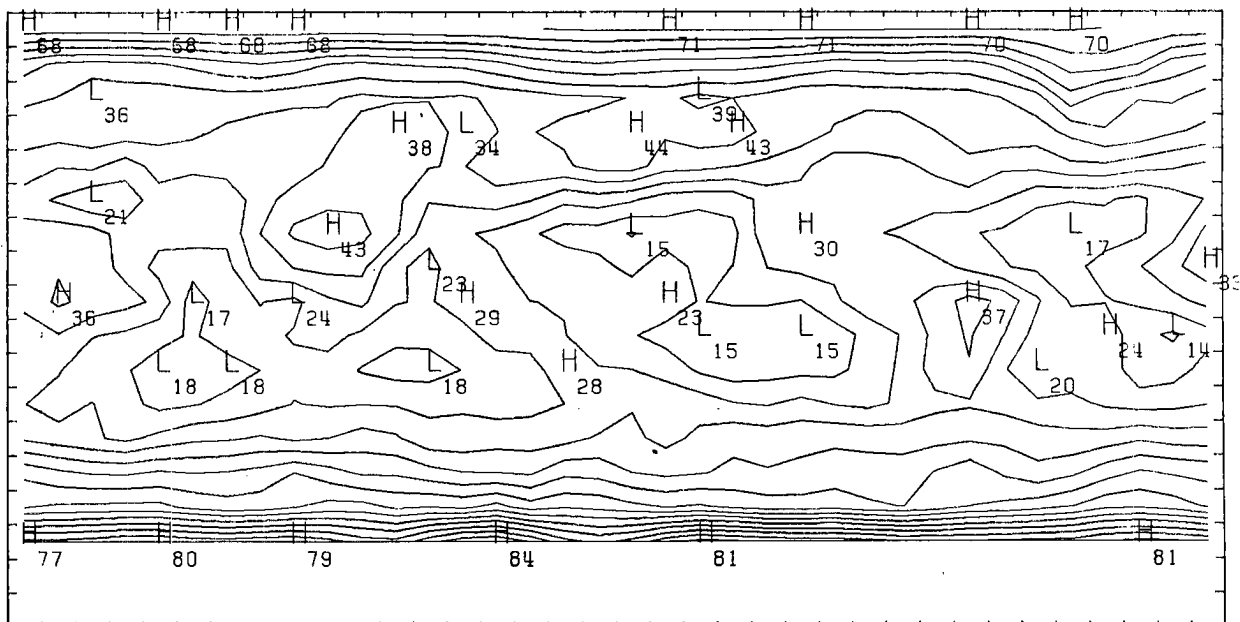
Net



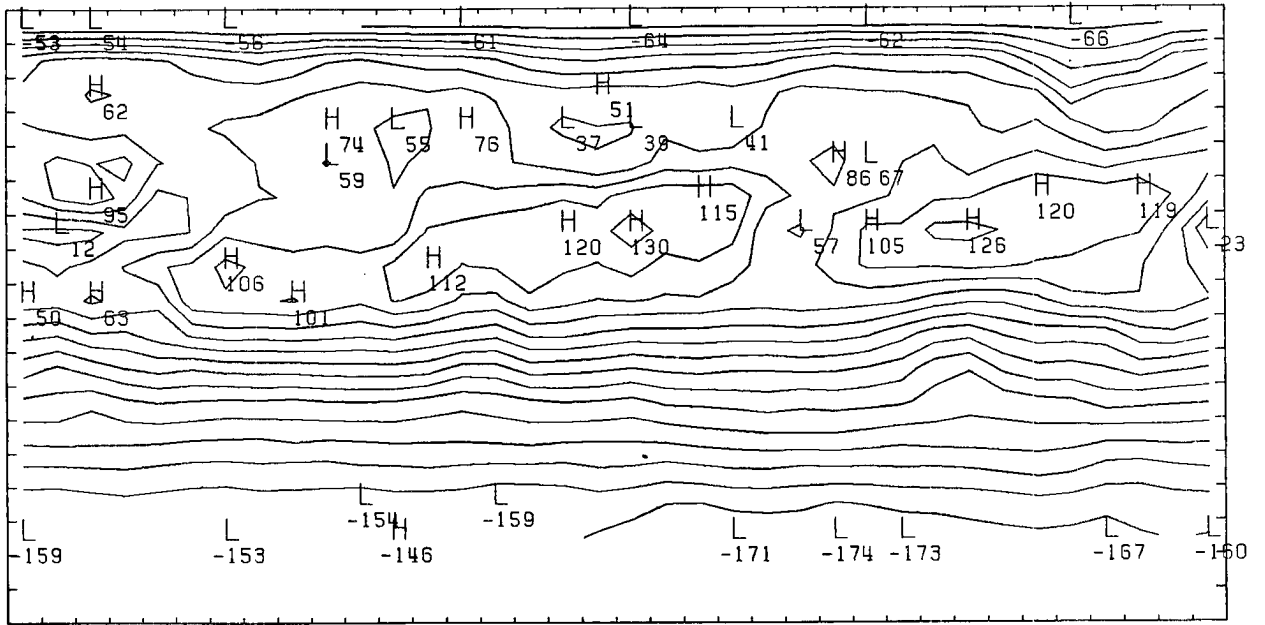
Emitted



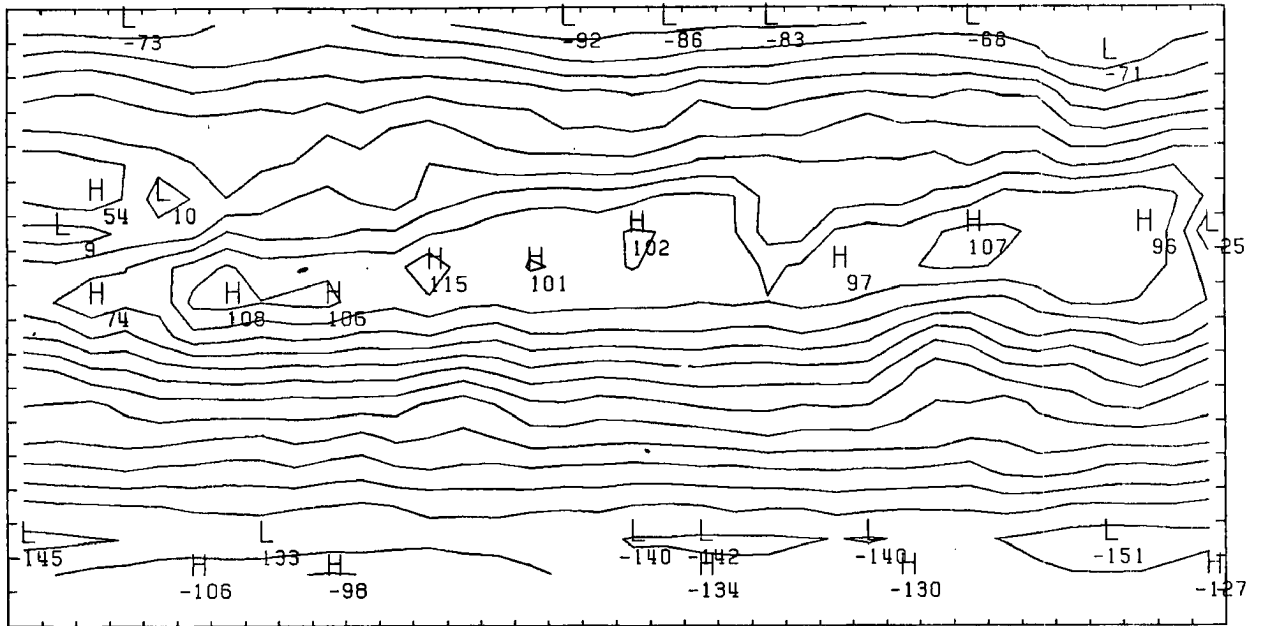
Albedo



Net

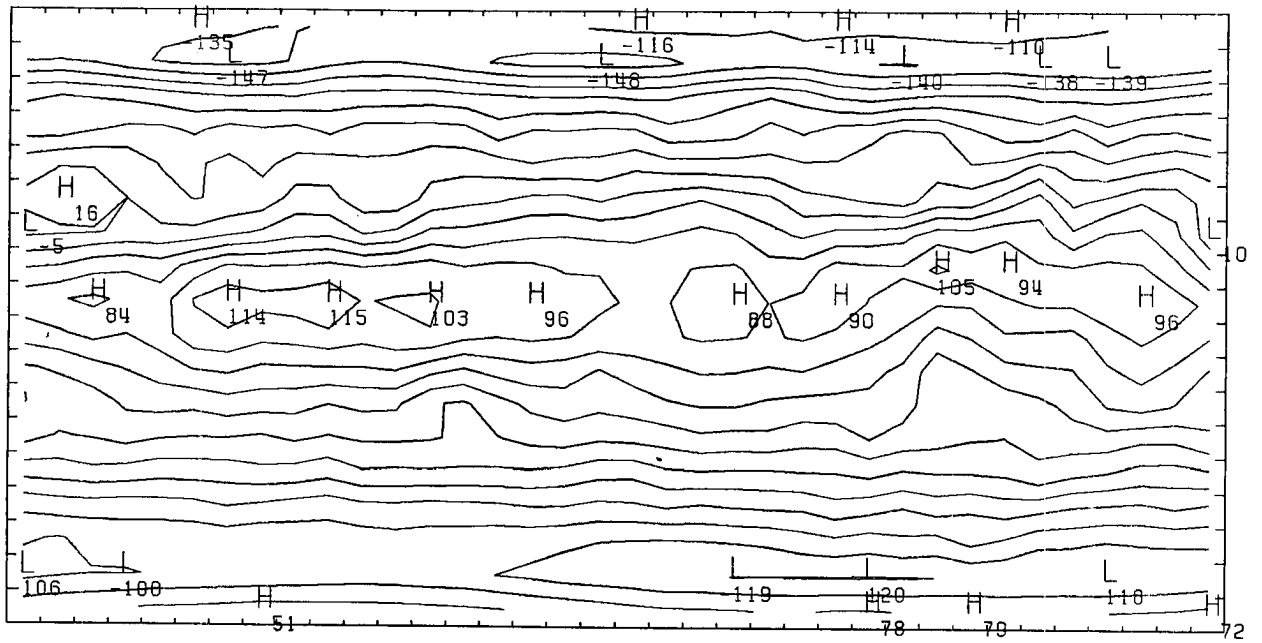


Net

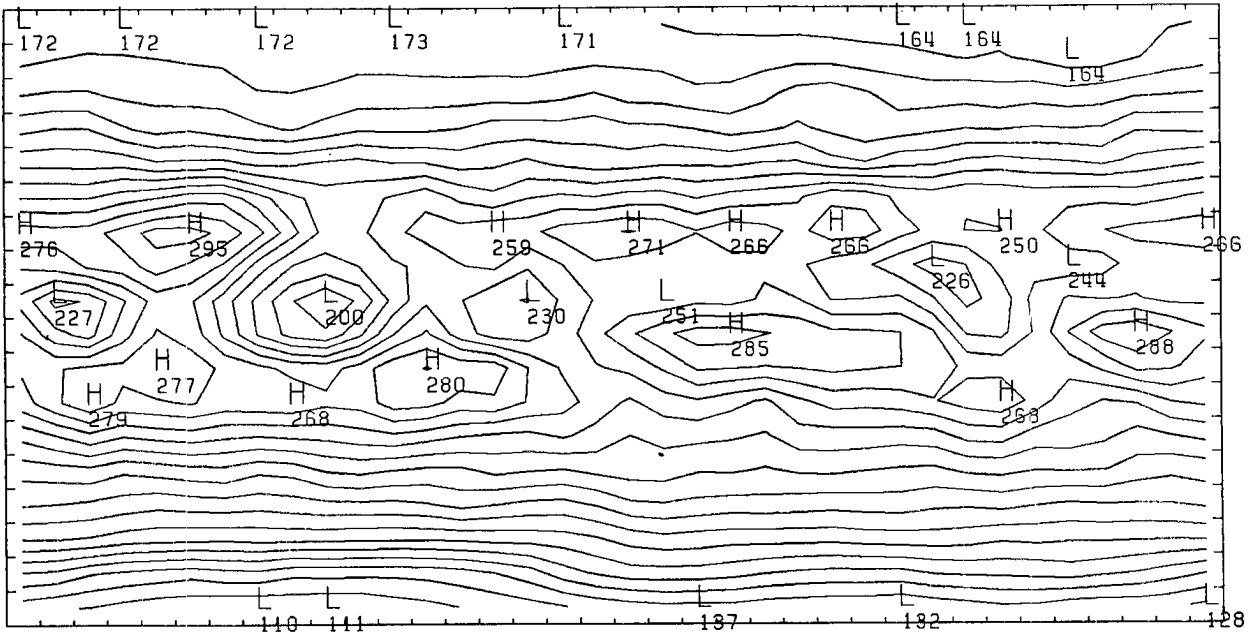


Map #10 September

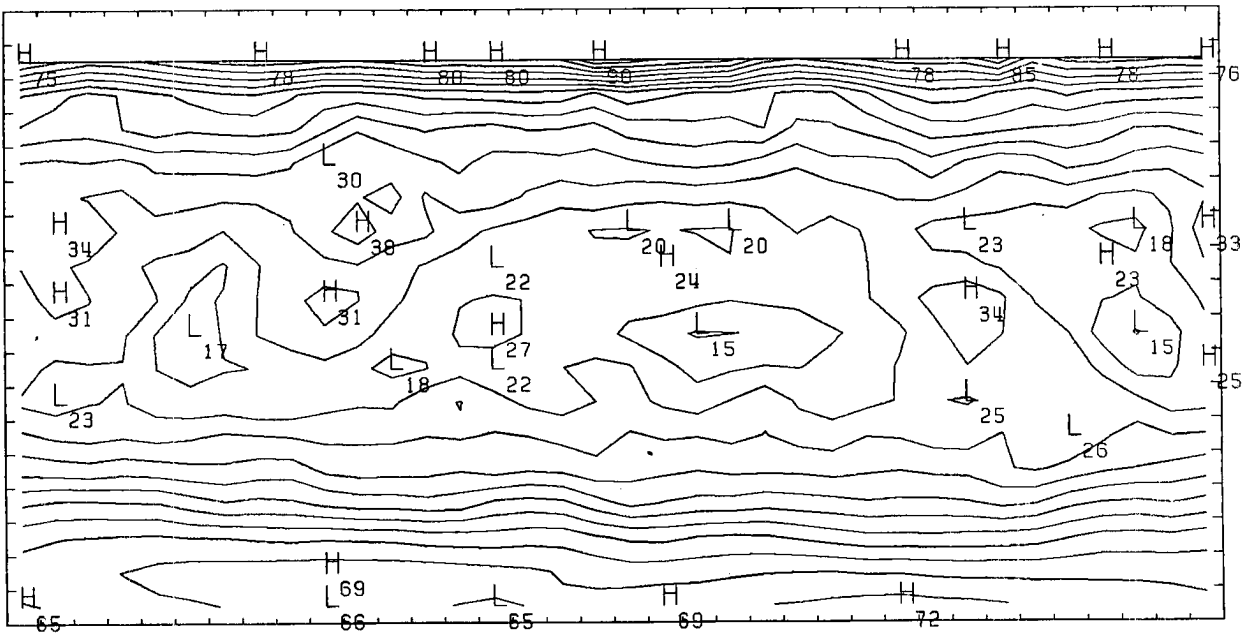
Net

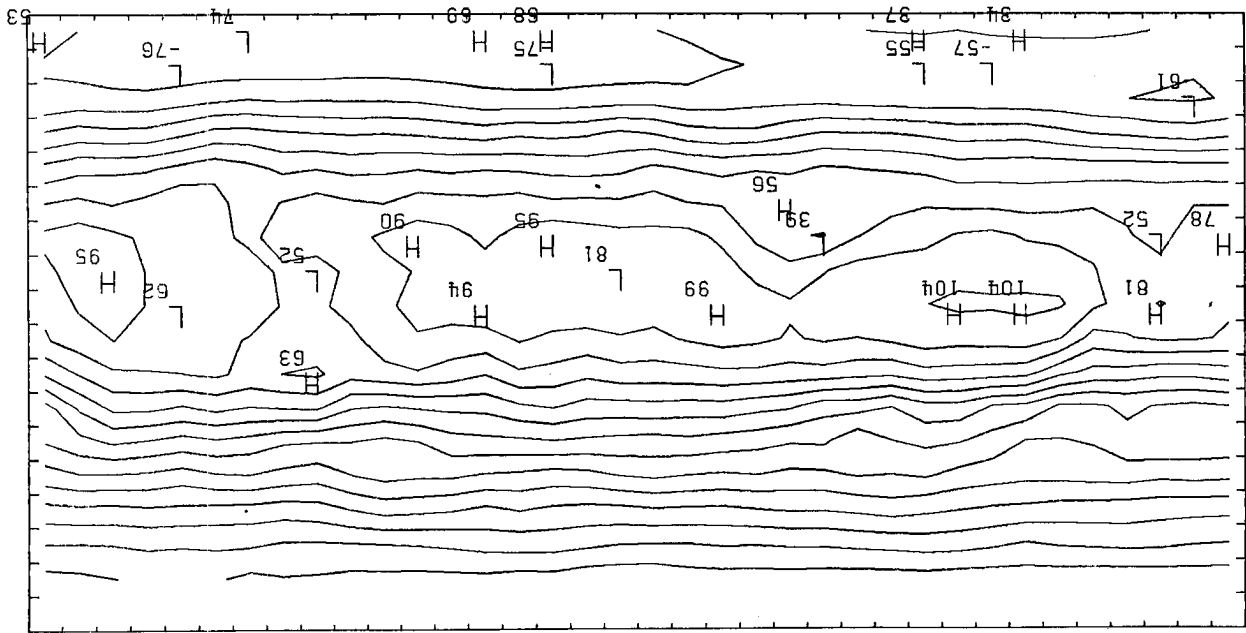


Emitted



Albedo

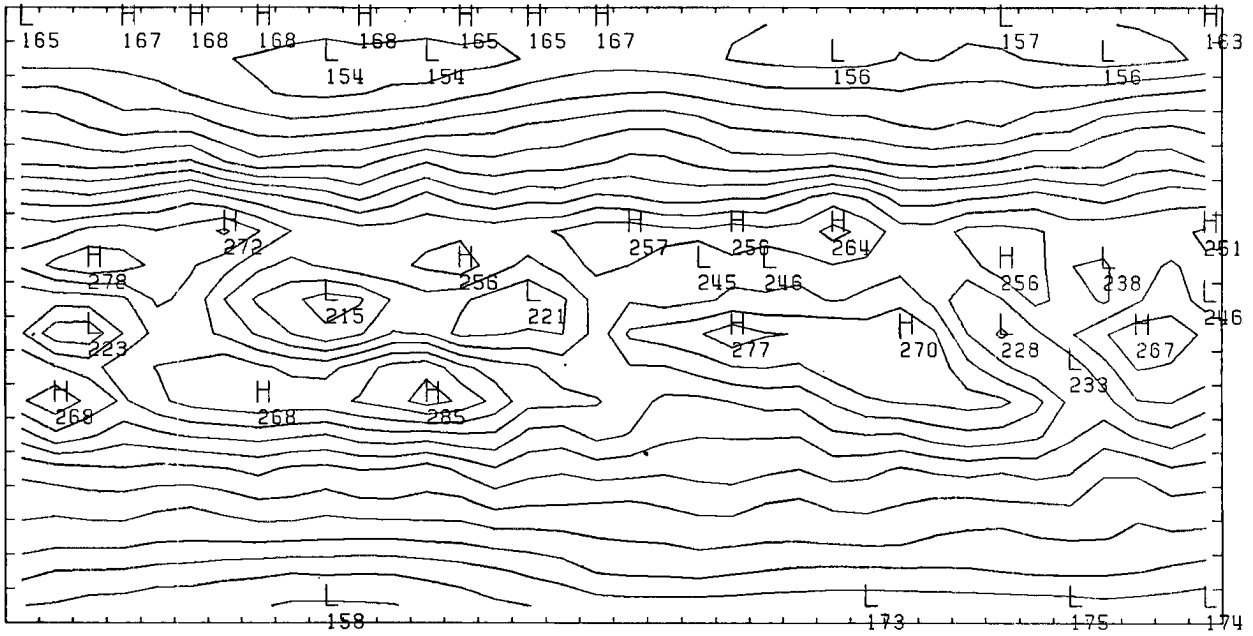




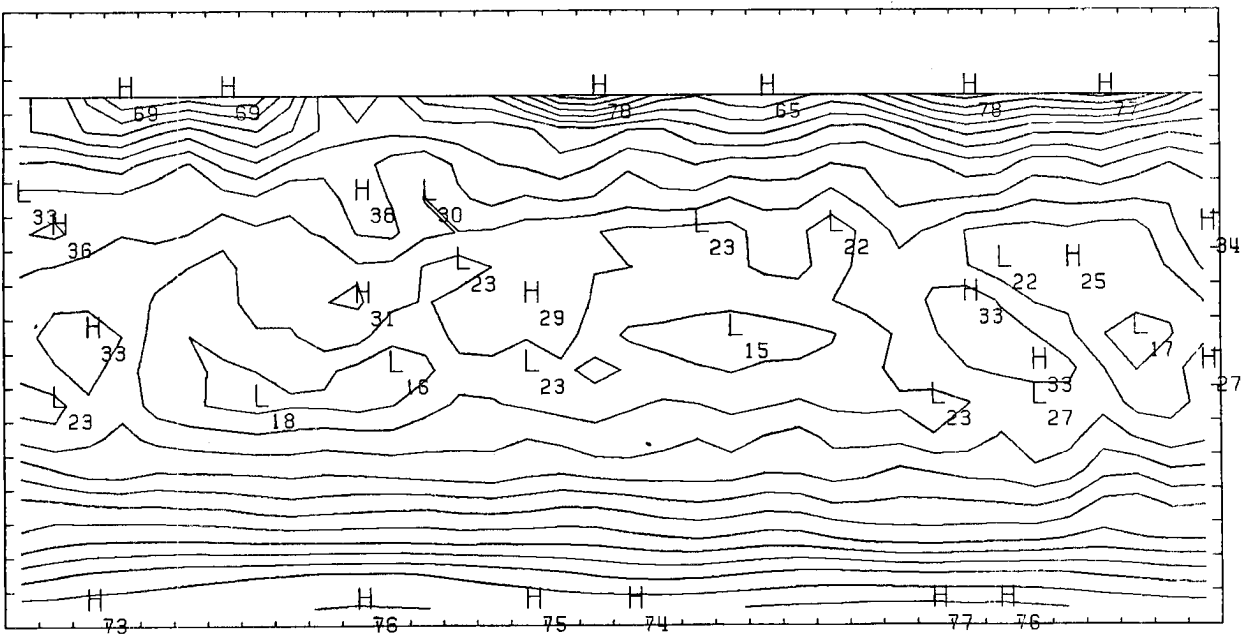
Net

Map #11 October

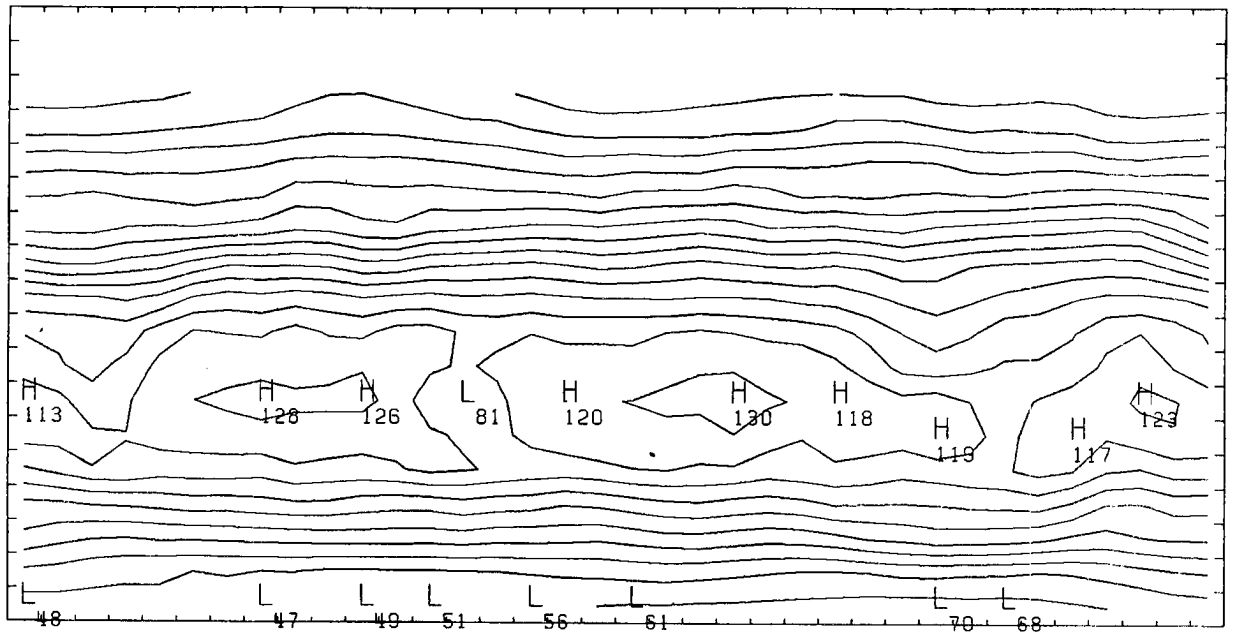
Emitted



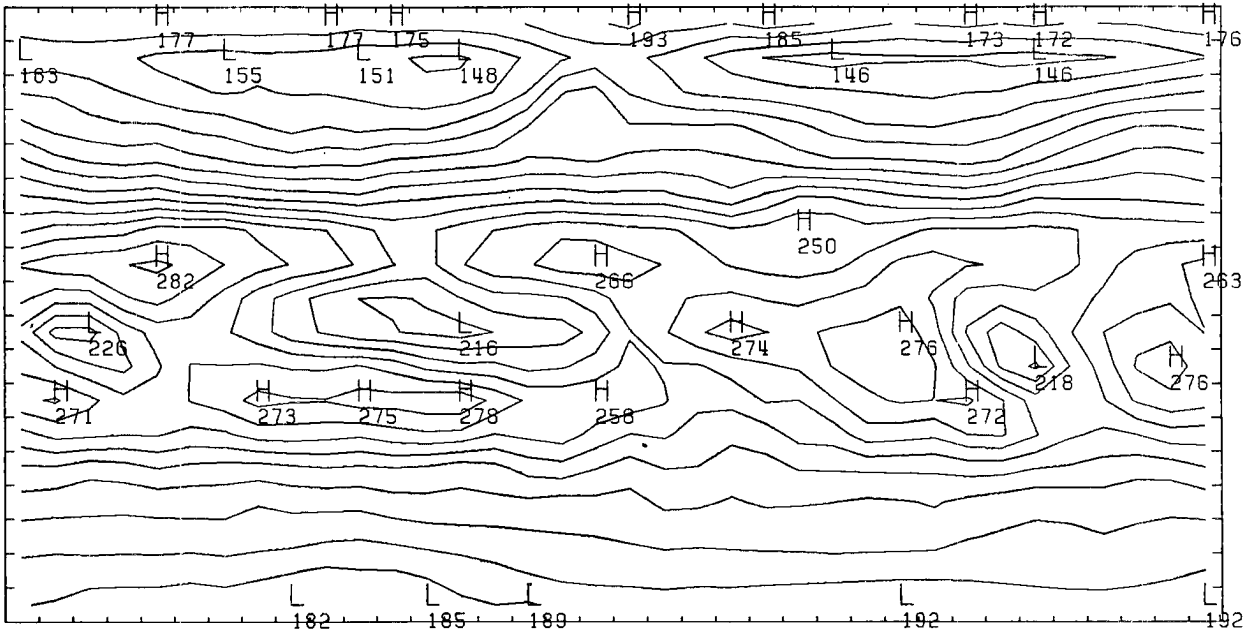
Albedo



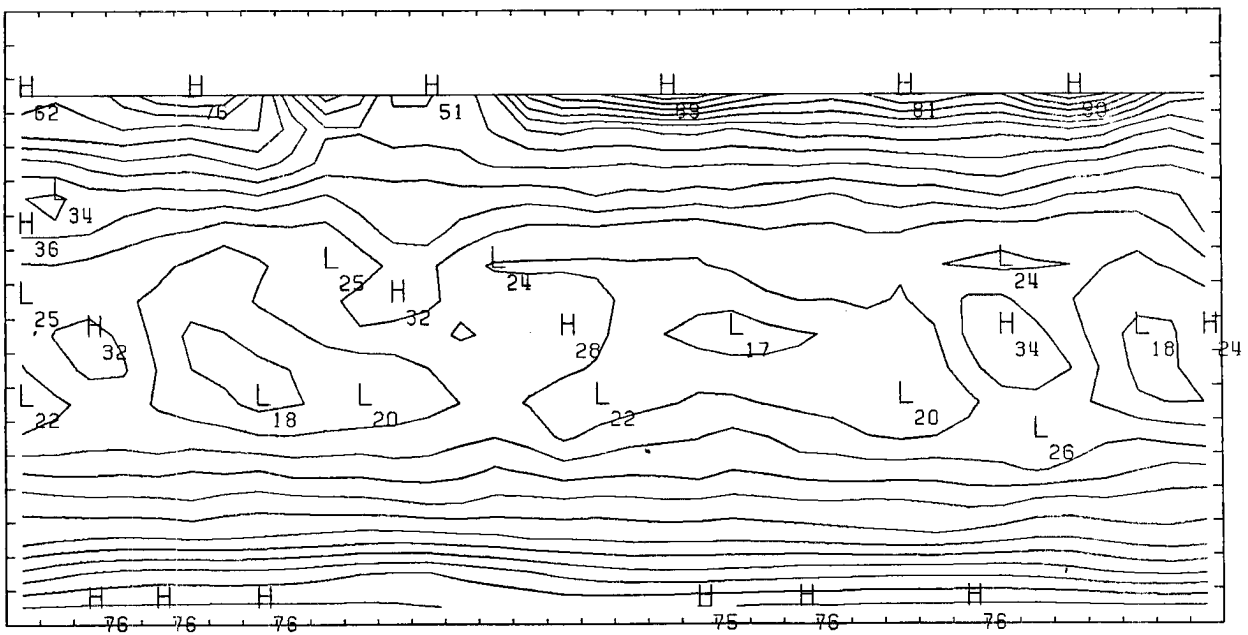
Net



Emitted

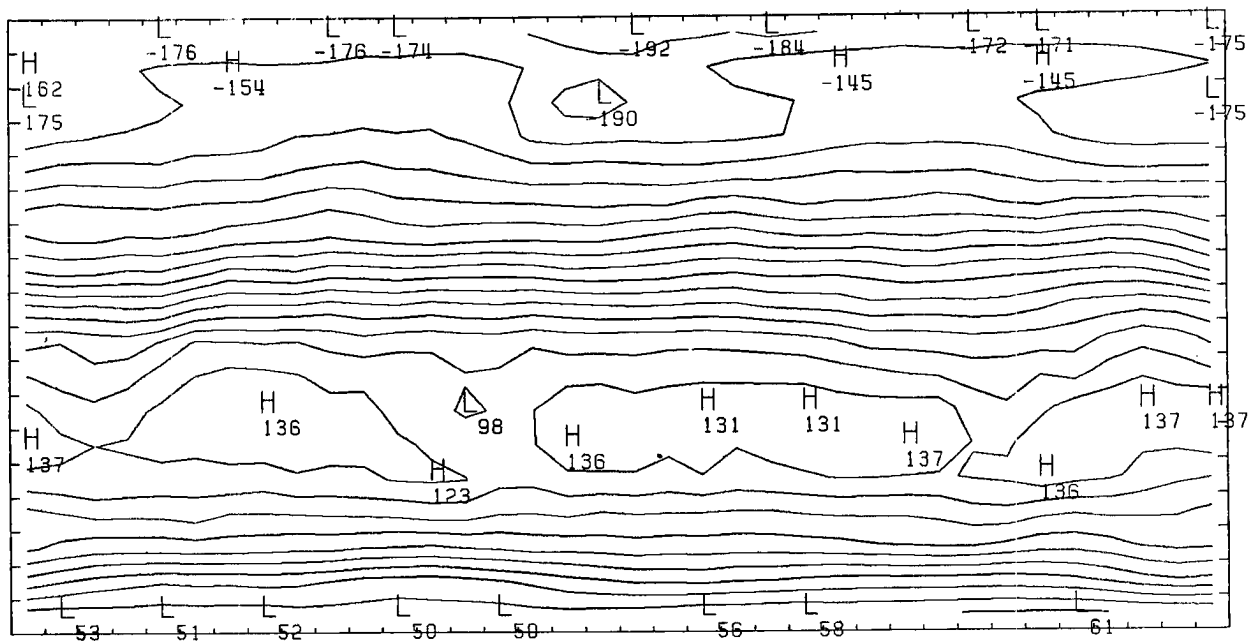


Albedo

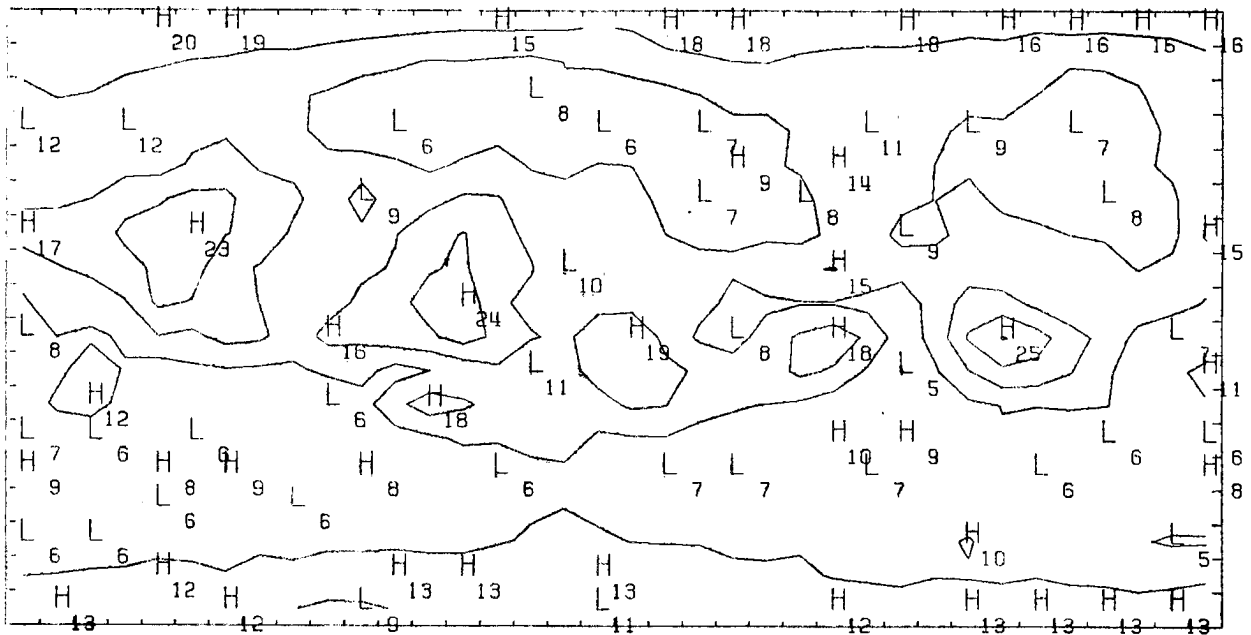


Map #13 December

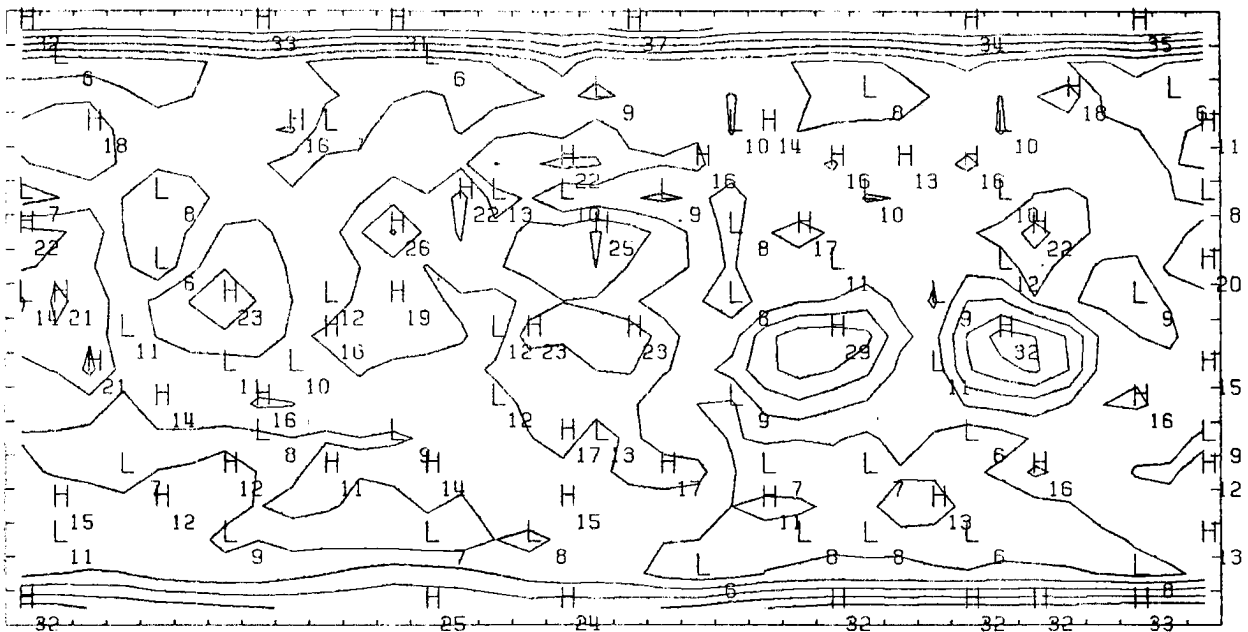
Net



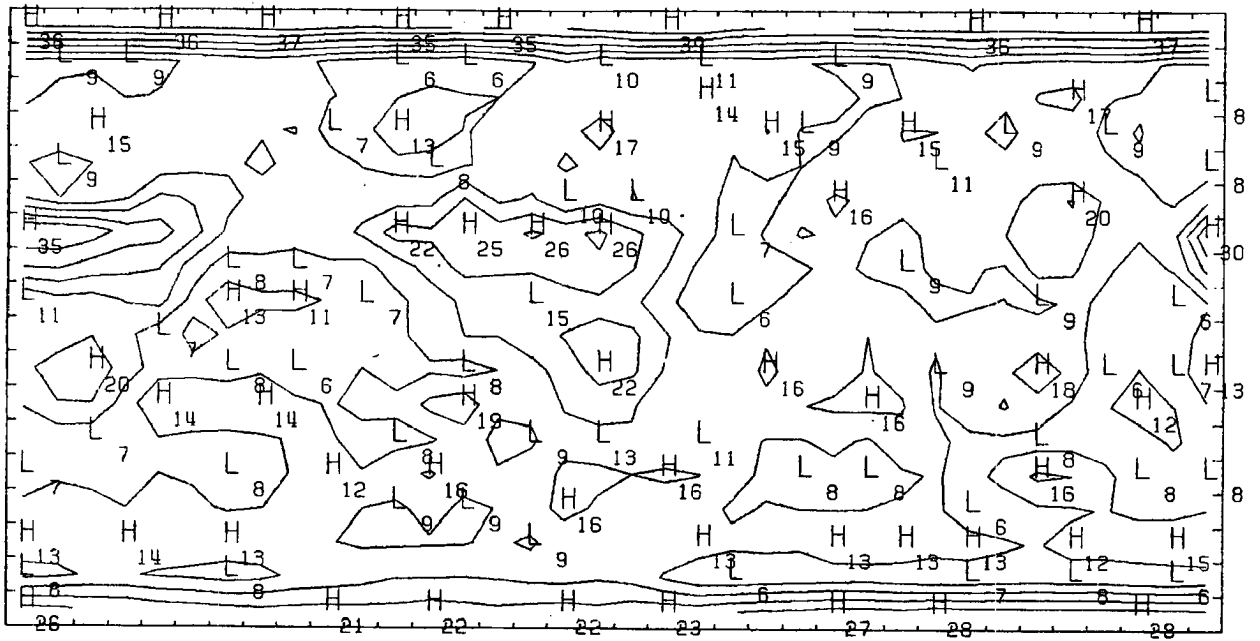
Map 14a
 Dispersion of Emitted W/m^2
 $\Delta = 5 W/m^2$



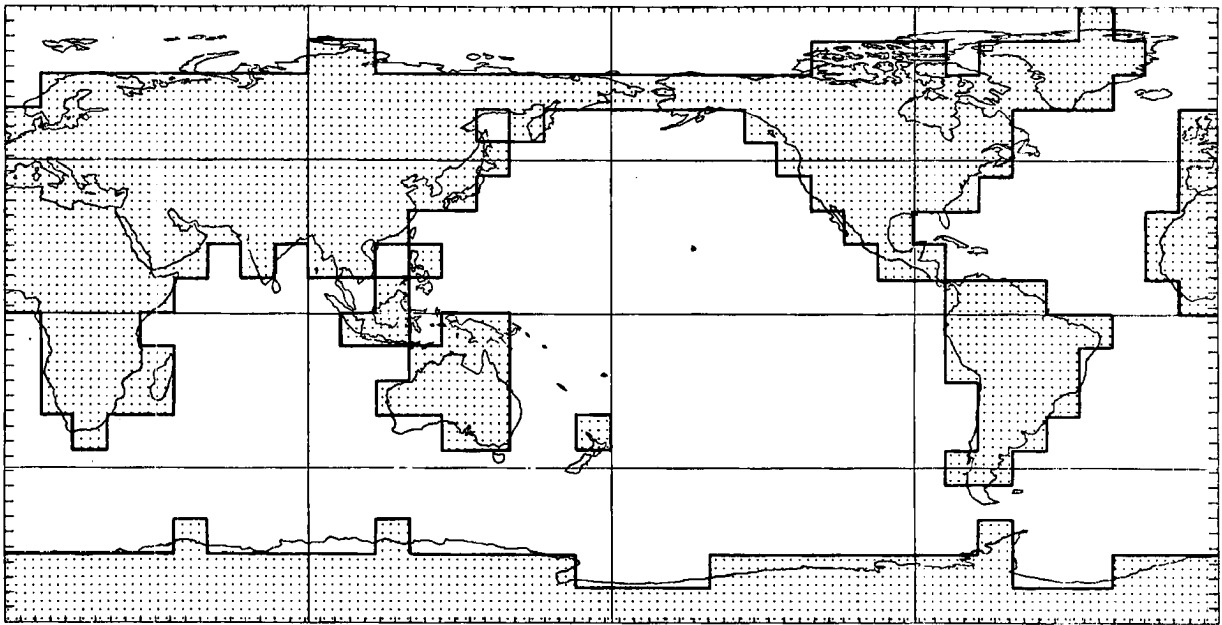
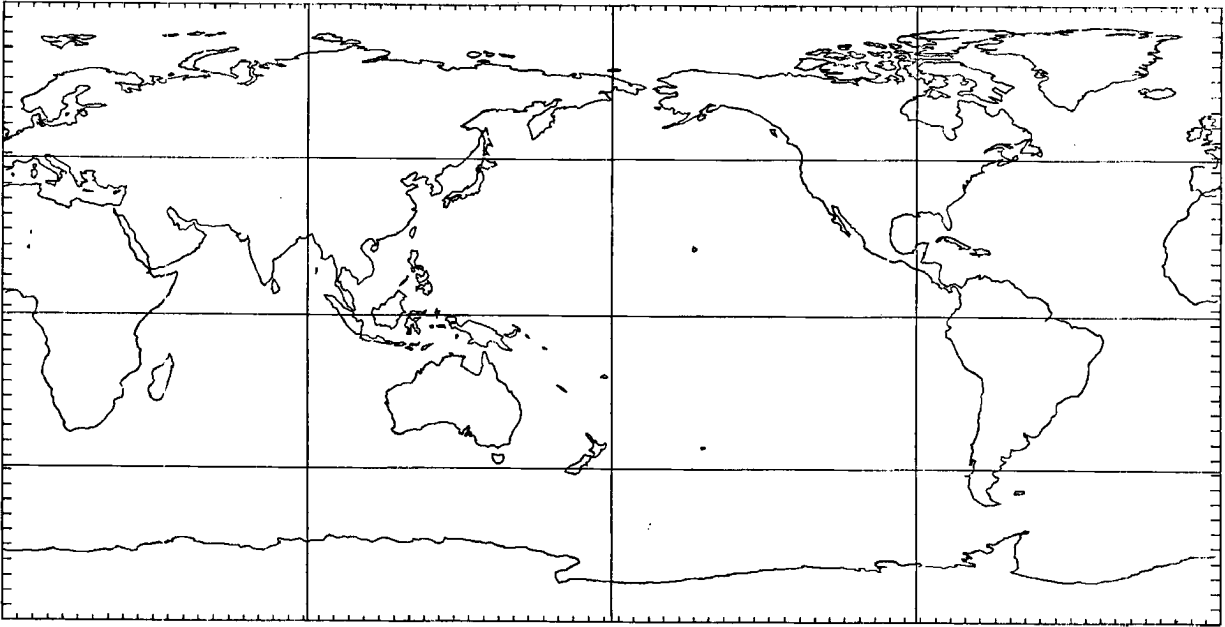
Map 14b
 Dispersion of Reflected W/m^2
 $\Delta = 5 W/m^2$



Map 14c
Dispersion of Net W/m^2
 $\Delta = 5 W/m^2$

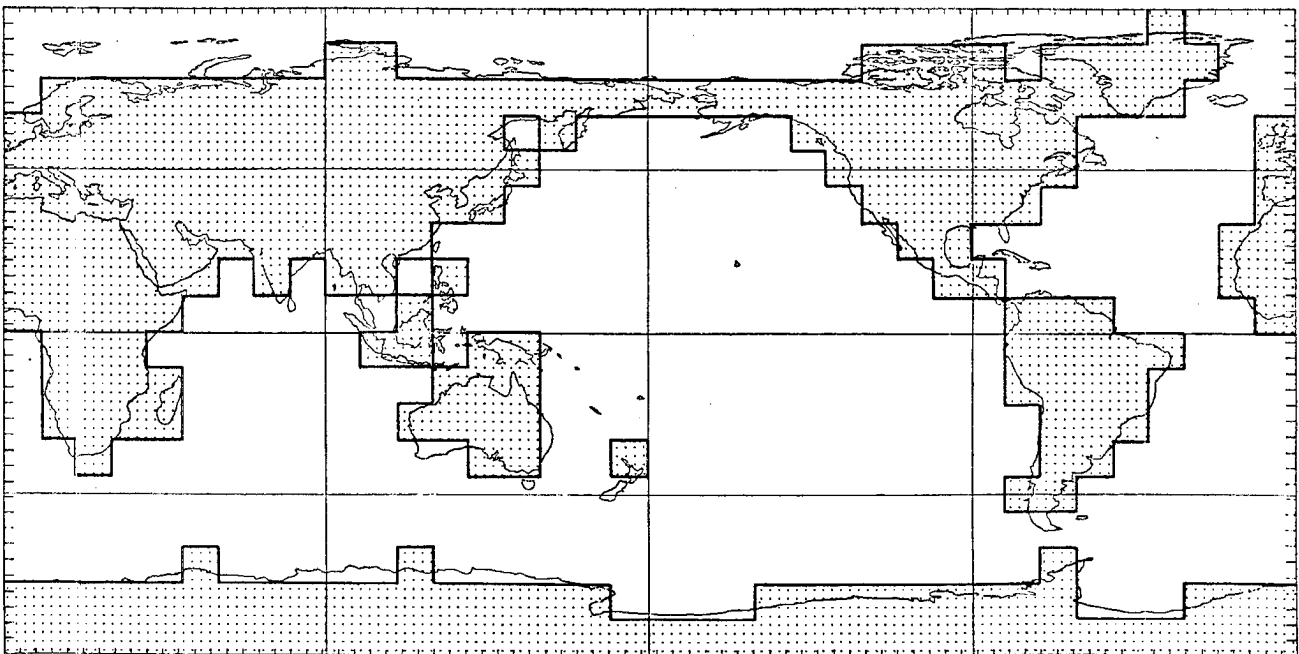
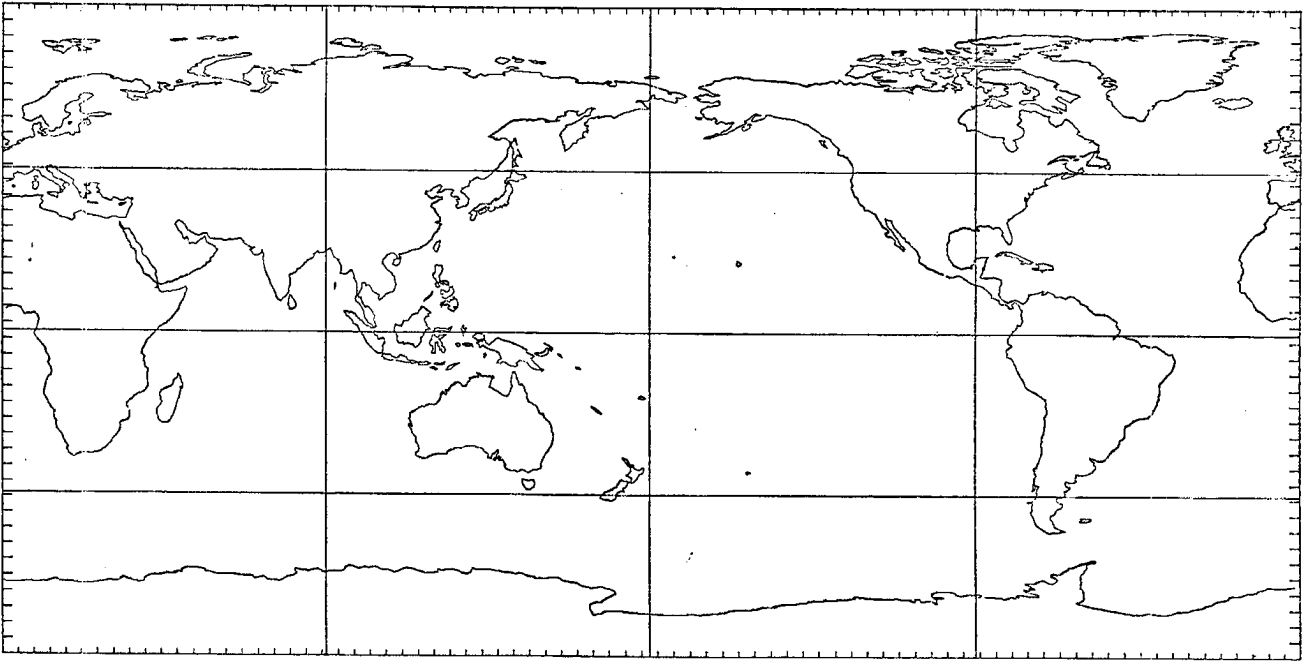


OVERLAY OF MAPS



Stippled regions were considered land for
the land, ocean zonal averages.

OVERLAY OF MAPS



Stippled regions were considered land for the land, ocean zonal averages.

REPORT DOCUMENTATION PAGE	1. REPORT NO. ATS PAPER NO. 323	2.	3. Recipient's Accession No.
4. Title and Subtitle Climatology of Radiation Budget Measurements from Satellites		5. Report Date February, 1980	
7. Author(s) G. G. Campbell and T. H. Vonder Haar		6.	
9. Performing Organization Name and Address Department of Atmospheric Science Colorado State University Ft. Collins, CO 80523		8. Performing Organization Rept. No. 323	
12. Sponsoring Organization Name and Address NASA NASA Headquarters 600 Independence Ave., S.W. Washington, D.C. 20233		10. Project/Task/Work Unit No.	
15. Supplementary Notes		11. Contract(C) or Grant(G) No. (C) NAS 5-22959 (G)	
16. Abstract (Limit: 200 words) Forty eight months of broadband earth radiation budget measurements have been accumulated into a climatology from satellite experiments. Monthly maps with 1100 km (10°) resolution are presented for the emitted flux, albedo and net radiation. The incident solar radiation is the prime determinant of the net radiation budget with land ocean distribution being the next significant factor. Mean cloudiness has an obvious effect on the mean net radiation only in a few places although cloud changes do have large effects on the albedo and emitted exitance. The zonal average ocean budget components are almost perfectly symmetric about the equator (with a six month shift). However, the land zonal average is much different than the ocean showing the need for consideration of land-ocean differences even in the simplest climate models. Several regional radiation budgets are discussed in detail.		13. Type of Report & Period Covered	
17. Document Analysis a. Descriptors Satellite observations Radiation budget of the earth Climate		14.	
b. Identifiers/Open-Ended Terms		15.	
c. COSATI Field/Group		16.	
18. Availability Statement: Unlimited	19. Security Class (This Report) Unclassified	21. No. of Pages 73	
	20. Security Class (This Page)	22. Price	